BIOCHEMISTRY
including biophysical chemistry & molecular biology

Article

pubs.acs.org/biochemistry

Impact of the Iron–Sulfur Cluster Proximal to the Active Site on the Catalytic Function of an O_2-Tolerant NAD^+-Reducing [NiFe]-Hydrogenase

Katja Karstens,[†] Stefan Wahlefeld,[‡] Marius Horch,[‡] Miriam Grunzel,[†] Lars Lauterbach,[†,‡] Friedhelm Lendzian,[‡] Ingo Zebger,[‡] and Oliver Lenz*[,†,‡]

[†]Institut für Biologie/Mikrobiologie, Humboldt-Universität zu Berlin, Chausseestr. 117, 10115 Berlin, Germany

[‡]Institut für Chemie, Sekr. PC14, Technische Universität Berlin, Straße des 17. Juni 135, 10623 Berlin, Germany

Supporting Information

ABSTRACT: The soluble NAD^+-reducing hydrogenase (SH) from *Ralstonia eutropha* H16 belongs to the O_2-tolerant subtype of pyridine nucleotide-dependent [NiFe]-hydrogenases. To identify molecular determinants for the O_2 tolerance of this enzyme, we introduced single amino acids exchanges in the SH small hydrogenase subunit. The resulting mutant strains and proteins were investigated with respect to their physiological, biochemical, and spectroscopic properties. Replacement of the four invariant conserved cysteine residues, Cys41, Cys44, Cys113, and Cys179, led to unstable protein, strongly supporting their involvement in the coordination of the iron–sulfur cluster proximal to the catalytic [NiFe] center. The Cys41Ser exchange, however, resulted in an SH variant that displayed up to 10% of wild-type activity, suggesting that the coordinating role of Cys41 might be partly substituted by the nearby Cys39 residue, which is present only in O_2-tolerant pyridine nucleotide-dependent [NiFe]-hydrogenases. Indeed, SH variants carrying glycine, alanine, or serine in place of Cys39 showed increased O_2 sensitivity compared to that of the wild-type enzyme. Substitution of further amino acids typical for O_2-tolerant SH representatives did not greatly affect the H_2-oxidizing activity in the presence of O_2. Remarkably, all mutant enzymes investigated by electron paramagnetic resonance spectroscopy did not reveal significant spectral changes in relation to wild-type SH, showing that the proximal iron–sulfur cluster does not contribute to the wild-type spectrum. Interestingly, exchange of Trp42 by serine resulted in a completely redox-inactive [NiFe] site, as revealed by infrared spectroscopy and H_2/D^+ exchange experiments. The possible role of this residue in electron and/or proton transfer is discussed.

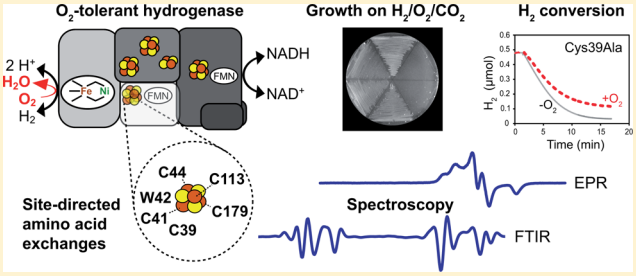

The *β*-proteobacterium *Ralstonia eutropha* H16 belongs to the phylogenetically diverse group of Knallgasbacteria, which are characterized by their capability to grow on H_2 and CO_2 as the sole energy and carbon sources, while O_2 is used as the terminal electron acceptor.[1] *R. eutropha* employs four distinct [NiFe]-hydrogenases, all of which are equipped with the rather unusual feature to split H_2 into electrons and protons in the presence of O_2. Research on the molecular grounds of O_2-tolerant H_2 cycling has gained increasing interest in the past decade from both fundamental and applied perspectives.[2−6] For instance, O_2-tolerant hydrogenases have already been used for light-driven hydrogen production,[7,8] enzymatic fuel cells,[9] and cofactor regeneration systems.[10]

Significant progress in the understanding of O_2 tolerance has recently been made for a subgroup of the so-called group 1 membrane-bound [NiFe]-hydrogenases. These enzymes possess a catalytic center composed of a nickel and an iron coordinated by four cysteine residues. Additionally, the iron carries two cyanide ligands and one carbon monoxide group. The most striking difference compared to O_2-sensitive [NiFe]-hydrogenases was found for the iron–sulfur cluster in the position proximal to the active site. Instead of a conventional [4Fe–4S] cluster, O_2-tolerant membrane-bound [NiFe]-hydrogenases carry an unprecedented [4Fe–3S] cluster coordinated by six cysteine residues. Several crystal structures[11−13] in combination with mutant studies[14,15] and spectroscopic investigations[14−20] have revealed that this cofactor is able to undergo two redox transitions instead of only one usually observed for [4Fe–4S] clusters. According to the current model, the capability of the [4Fe–3S] cluster to store two electrons at a time enables a rapid delivery of electrons toward the active site in case of O_2 attack, thereby assisting in the complete reduction of O_2 to harmless water.[6,21]

The hypothesis that water represents the main product of O_2 reduction during H_2 cycling under aerobic conditions has recently been verified on the basis of experiments performed with the NAD^+-reducing soluble [NiFe]-hydrogenase (SH) from *R. eutropha* and hydrogenase-1 from *Escherichia coli*.[22,23]

Received: October 29, 2014
Revised: December 16, 2014
Published: December 17, 2014

DOI: 10.1021/bi501347u
Biochemistry 2015, 54, 389−403

The SH couples H_2 oxidation with the reduction of NAD^+ and represents a well-studied representative of the bidirectional heteromultimeric cytoplasmic [NiFe]-hydrogenases, subsumed in group 3 according to the classification by Vignais and Billoud.[24] More precisely, the SH together with the bidirectional hydrogenases from cyanobacterial species forms the subgroup of pyridine nucleotide-dependent [NiFe]-hydrogenases (group 3d). These enzymes are basically composed of a NAD(P)H:acceptor oxidoreductase module, consisting of the subunits HoxF and HoxU, and a hydrogenase module, which comprises a large, active site-containing subunit (HoxH) and a small subunit (HoxY) harboring one iron−sulfur cluster (Figure 1).[25−28] The cyanobacterial representatives have been proposed to function as an electron valve, as they produce H_2 from accumulating reducing equivalents under anaerobic conditions.[29,30] Notably, cyanobacterial hydrogenases are inactivated by O_2 but can be reactivated under reducing conditions, as recently shown for the enzyme from *Synechocystis* sp. PCC 6803.[31] This is in marked contrast to the *R. eutropha* SH, which has been shown to maintain its catalytic activity even in the presence of high O_2 levels.[22,32,33] The SH has been shown to oxidize H_2 during aerobic lithoautotrophic growth of *R. eutropha*[34] and to produce H_2 in the transition phase from aerobic and anaerobic growth.[35] In addition to the core subunits HoxFUYH, the SH accommodates two copies of the HoxI protein (Figure 1).[36] According to recent FTIR studies, the hydrogenase large subunit HoxH contains a [NiFe] active site in which the iron is equipped with one CO and two CN^- ligands.[28,37,38] The small hydrogenase subunit HoxY represents a C-terminally truncated version of canonical hydrogenase small subunits that contain three iron−sulfur clusters. Only the Fe−S cluster in position proximal to the active site seems to be conserved in HoxY (Figure 1). Its presence has been confirmed by metal determination as well as UV/vis and X-ray absorption spectroscopy, suggesting a [4Fe−4S] species.[28] In addition to a Fe−S cluster, the HoxY subunit has been described to contain a weakly bound flavin mononucleotide (FMN) cofactor (FMN-a) (Figure 1).[28,39,40] The NADH:acceptor oxidoreductase module HoxFU of the SH harbors another FMN cofactor (FMN-b) and binding motifs for three [4Fe−4S] clusters and

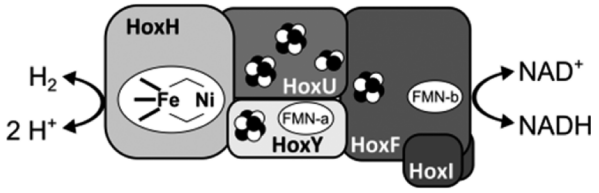

Figure 1. Model of the soluble, NAD^+-reducing [NiFe]-hydrogenase from *R. eutropha* H16. The subunits of the hydrogenase module (HoxH/HoxY) and the NADH:acceptor oxidoreductase module (HoxF/HoxU/$HoxI_2$) are depicted with their postulated cofactors, including the [NiFe] active site, FMN cofactors, and Fe−S centers.

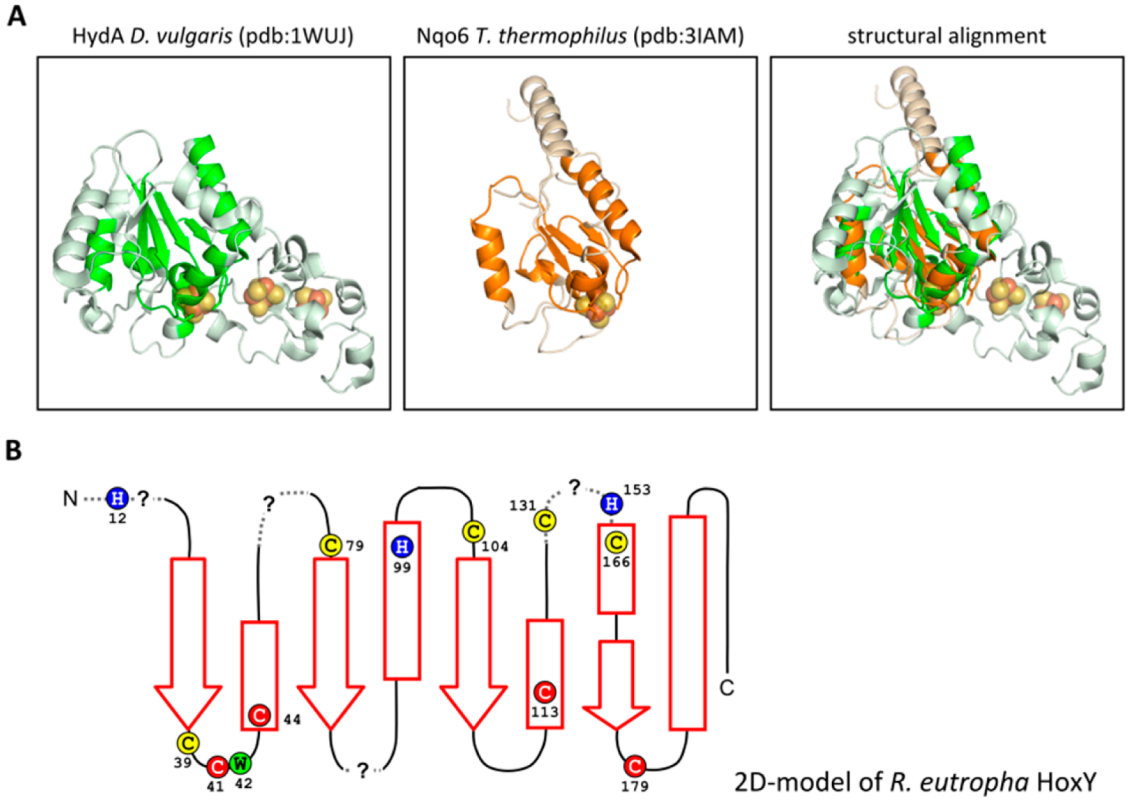

Figure 2. Model of the *R. eutropha* HoxY secondary structure based on crystal structures of homologous proteins. (A) Superposition of the crystal structures of the small subunit of a group 1 [NiFe]-hydrogenase and the Nqo6 subunit of Complex I. Conserved structural elements are marked by bright colors. Iron−sulfur clusters are shown as spheres. (B) Topology model of HoxY from *R. eutropha* based on the sequence alignment with HydA and Nqo6. HoxY stretches that do not possess counterparts in the crystal structures are indicated by question marks. The colored amino acids were exchanged in this study. Cysteine residues marked in red are highly conserved and supposed to coordinate a [4Fe−4S] cluster. Cysteines, histidine, and tryptophan residues marked in yellow, blue, and green, respectively, are exclusively found in group 3 [NiFe]-hydrogenases that are presumed to be O_2-tolerant (see Figure S1 for a multiple-sequence alignment).

DOI: 10.1021/bi501347u
Biochemistry 2015, 54, 389−403

one [2Fe−2S] cluster, which is in accordance with spectroscopic results, metal determination, and the similarity of the SH with the peripheral arm of Complex I.[27] Inspection of the H_2-reduced enzyme by EPR confirmed the presence of the $[2Fe-2S]^+$ cluster. In contrast, EPR signals corresponding to only one $[4Fe-4S]^+$ cluster were observed. Genetic engineering in combination with protein biochemistry and spectroscopic experiments suggest that the Fe−S cluster in the HoxY subunit is indeed EPR-silent.[28,32,38,41,42] The four highly conserved cysteines, C41, C44, C113, and C179, in the HoxY subunit could serve as ligands for a [4Fe−4S] cluster. However, the HoxY subunits of SH representatives that have been shown or are supposed to be O_2-tolerant contain a number of cysteine and histidine residues that are not present in the O_2-sensitive cyanobacterial counterparts (Figures S1 and 2). To investigate the role of these residues in the catalytic function and O_2 tolerance of the SH, we exchanged them by site-directed mutagenesis (Figure 2). Moreover, aromatic amino acids have been shown to assist in binding of the flavin cofactor by $\pi-\pi$ stacking interactions, e.g., in monooxygenases.[43] Indeed, a tryptophan residue (W42) is located in close proximity to the proposed [4Fe−4S] cluster in HoxY. To elucidate the possible role of this residue in the stabilization of FMN-a, we substituted W42 with serine, which is found at the corresponding position in O_2-sensitive SH homologues. The resulting mutant strains and purified SH variants were analyzed systematically with the aid of physiological, biochemical, and spectroscopic methods.

MATERIALS AND METHODS

Bacterial Strains and Plasmids. All strains used in this study are listed in Table 1. Plasmids used for the construction of these strains can be found in Table S1. *Escherichia coli* strains JM109 and XL1-Blue were used as hosts for standard cloning procedures. *E. coli* S17-1 was used as donor for conjugative plasmid transfer to *R. eutropha* H16 derivatives via spot mating.[44] Derivatives of the suicide plasmid pLO3 were used for allelic exchanges in *R. eutropha* strains based on double homologous recombination.[45]

A 969 bp PshAI/Ecl136II fragment of pCH#2904 containing *5′-UTR$_{hoxF}$-strep-hoxF′* was cloned into PmeI-digested pLO3. The resulting plasmid, pCH1655, was used to replace the wild-type *hoxF* allele in *R. eutropha* strain HF869, which synthesized exclusively the SH because the large subunit genes of the remaining hydrogenases (MBH, RH, and AH) have been deleted on the H16-specific megaplasmid pHG1. The resulting strain, *R. eutropha* HF1009 (SH^+, MBH^-, RH^-, and AH^-), encodes a *Strep*-tagged version of the wild-type SH and served as the basis for construction of 20 derivatives encoding SH variants with single amino acid exchanges in HoxY. To introduce the single amino acid exchanges, a pCH#2904-derived 936 bp AgeI/SacI fragment carrying *hox′UY′* was cloned into AgeI/SacI-digested Litmus 29, yielding pCH1617. The plasmid pCH1617 was used as template for site-directed mutagenesis using the QuikChange protocol and the mutagenic primers listed in Table S2. Introduction of the desired mutations in resulting plasmids pCH1618−pCH1635 and pCH1643 was verified by sequencing. Subsequently, 978 bp SacI/PstI fragments carrying the mutagenized *hox′UY′* region were cloned into SacI/PstI-cut pLO3, resulting in pCH1657−pCH1663, pCH1665−pCH1674, and pCH1648. The 1068 bp StuI/SnaBI fragment of pCH1618 was ligated into the PmeI-digested pLO3 vector, resulting in pCH1656. The pLO3 derivatives were used for gene replacement in *R. eutropha* HF1009, yielding the *R. eutropha* mutant strains HF1010−HF1017, HF1019−HF1028, and HF1030.

Table 1. Bacterial Strains Used in This Study

strain	relevant characteristics	ref
Ralstonia eutropha		
HF869	pHG1^{+a} with Δ*hoxG*, Δ*hoxC*, Δ*hofG* (SH^+, MBH^-, RH^-, AH^-)	C. Schäfer and O. Lenz, unpublished
HF210	pHG1$^-$ (SH^-, MBH^-, RH^-, AH^-)	73
HF1009	derivative of HF869 with *strep-hoxF*, *hoxY*^{WT}	this study
HF1010	derivative of HF1009 with *hoxY*^{H12E}	this study
HF1011	derivative of HF1009 with *hoxY*^{H99E}	this study
HF1012	derivative of HF1009 with *hoxY*^{H153E}	this study
HF1013	derivative of HF1009 with *hoxY*^{C39G}	this study
HF1014	derivative of HF1009 with *hoxY*^{C79V}	this study
HF1015	derivative of HF1009 with *hoxY*^{C104S}	this study
HF1016	derivative of HF1009 with *hoxY*^{C131V}	this study
HF1017	derivative of HF1009 with *hoxY*^{C166V}	this study
HF1019	derivative of HF1009 with *hoxY*^{C39A}	this study
HF1020	derivative of HF1009 with *hoxY*^{C39S}	this study
HF1021	derivative of HF1009 with *hoxY*^{C41G}	this study
HF1022	derivative of HF1009 with *hoxY*^{C41S}	this study
HF1023	derivative of HF1009 with *hoxY*^{C44G}	this study
HF1024	derivative of HF1009 with *hoxY*^{C44S}	this study
HF1025	derivative of HF1009 with *hoxY*^{C113G}	this study
HF1026	derivative of HF1009 with *hoxY*^{C113S}	this study
HF1027	derivative of HF1009 with *hoxY*^{C179G}	this study
HF1028	derivative of HF1009 with *hoxY*^{C179S}	this study
HF1030	derivative of HF1009 with *hoxY*^{W42S}	this study
Escherichia coli		
JM109	*recA1 endA1 gyrA96 thi hsdR17*($r_K^-m_K^+$) *relA1 supE44* Φ*80*Δ*lacZ* Δ*M15* Δ*(lacZYA-argF)U169*	74
XL1-Blue	*Tc^r; recA1 endA1 gyrA96 thi hsdR17*($r_K^-m_K^+$) *relA1 supE44 lac*(F′[*proAB lacI^q lacZ*Δ*M15* Tn*10*])	Stratagene
S17-1	Strep^{r}Tp^r; *recA1 pro thi hsdR17*($r_K^-m_K^+$); harbors the RP4-2 *tra* genes in the chromosome	44

[a]Megaplasmid pHG1 carries all hydrogenase-related genes of *R. eutropha* H16.

Media and Growth Conditions. *E. coli* was grown in lysogeny broth (LB) at 37 °C. Ampicillin and tetracycline were used at final concentrations of 100 and 20 μg mL^{-1}, respectively. *R. eutropha* was grown in nutrient broth (NB), low salt LB (LSLB), or minimal medium with 0.2% (w/v) fructose (FN), described previously,[46] at 37 °C. Tetracycline was used at a final concentration of 15 μg mL^{-1}. Screening on LSLB-sucrose plates was performed at a concentration of 20% (w/v) sucrose. For SH expression, *R. eutropha* strains were grown in FGN* medium under O_2-limiting conditions in 80% (v/v)-filled baffled flasks at 30 °C as described previously.[14] FGN* medium contained 0.05% (w/v) fructose, 0.4% (w/v) glycerol, 0.2% (w/v) ammonium chloride, 0.2% (w/v) $MgSO_4$, 0.001% (w/v) $CaCl_2 \cdot 2H_2O$, 0.001% (w/v) $FeCl_3 \cdot 6H_2O$, 1 μM $NiCl_2$, 25.1 mM Na_2HPO_4, and 11 mM KH_2PO_4, pH 7.0, and was additionally supplemented with 1 μM $ZnCl_2$ and 0.1% (v/v) trace element mixture (10× SL6 without Ni^{2+}).[47] Baffled Erlenmeyer flasks with a total volume of 500 and 250 mL were filled with 400 and 200 mL medium, respectively. For large-scale enzyme preparation for spectroscopic analysis, cultures were grown in baffled 5 L flasks filled with 4 L of media. An exception was strain *R. eutropha* HF1022 (SH^{C41S}), which

DOI: 10.1021/bi501347u
Biochemistry 2015, 54, 389−403

produced more active protein when cultivated on the 400 mL scale. Cells were harvested after 6−12 days at an optical density at 436 nm ranging between 9 and 13.

Lithoautotrophic cultures were grown on solid mineral medium based on the recipe described above for SH production and 1.5% (w/v) bacto agar but without an organic carbon source. The agar plates were incubated for 5−7 days at 30 °C under an atmosphere of 10% (v/v) CO_2, 3% (v/v) H_2, x % (v/v) O_2, and (87 − x)% (v/v) N_2.

Enzyme Purification. Enzyme purification was generally performed at 4 °C under aerobic conditions. For small-scale purification, ∼1.5 g of cells (wet weight) was resuspended in 2.5 mL of SH6 buffer (50 mM K-PO_4, pH 7.1, 5% (v/v) glycerol, EDTA-free protease inhibitor (Roche)) containing 5 mM NAD^+. The cells were disrupted by two passages through a chilled French pressure cell (SLM Aminco) at 1.10×10^5 kPa. The crude extract was fractionated by ultracentrifugation at 100 000g for 45 min. The supernatant, termed soluble extract, was applied twice to a *Strep*-Tactin column (0.5 mL *Strep*-Tactin Superflow matrix (IBA, Göttingen, Germany) in a 2.5 mL MoBiTec column (MoBiTec, Göttingen, Germany)), which was previously equilibrated with SH6 buffer + 5 mM NAD^+. After washing the column with 4 volumes of SH6 buffer + 5 mM NAD^+ and 6 volumes of SH6 buffer, the *Strep*-tagged SH protein was eluted with up to 10 volumes of SH6 buffer containing 5 mM desthiobiotin. The pooled elution factions were then concentrated with a centrifugal filter device (Amicon Ultra-15, 100K, Millipore, Molsheim, France), and the buffer was subsequently exchanged to SH6 buffer using the same device. For large-scale purifications, cell suspensions (grams of cells (wet weight)/mL SH6 buffer: SH^{WT}, SH^{C39G}, and SH^{C39S}, 15:20; SH^{C41S} and SH^{W42S}, 40:50) were disrupted by two passages through a chilled French pressure cell (G. Heinemann, Schwäbisch Gmünd, Germany) at 1.24×10^5 kPa. Portions of 10−20 mL of the soluble extract were applied to *Strep*-Tactin columns with 1 to 2 mL matrix volumes. Purification was done as described above. Centrifugal filter devices (Amicon Ultra-0.5, 50K) were used for concentrating the protein samples to volumes below 200 μL. Aliquots of the purified proteins were frozen in liquid nitrogen and stored at −80 °C.

H_2-Dependent NAD^+ Reduction Assay. H_2-dependent NAD^+ reduction was assayed at 30 °C in H_2-saturated 50 mM Tris/HCl buffer (pH 8.0) containing 1 mM NAD^+.[25] The following supplements (final concentration) were added to the reaction mixture when indicated: flavin mononucleotide (FMN, 1 μM), dithiothreitol (DTT, 1 mM), Tris(2-carboxyethyl)-phosphine (TCEP, 1 mM), and β-mercaptoethanol (β-EtSH, 1 mM). Soluble extracts were prepared as described for protein purification but with 50 mM K-PO_4 buffer, pH 7.0, and analyzed the same day. A previously described protocol was used for whole-cell activity measurements.[48] Cells were lysed with cetyltrimethylammonium bromide (CTAB), and the protocol was adapted to a 2 mL scale with an initial concentration of 1 mM NAD^+. The final optical density (OD_{436}) in the assay lay between 0.15 and 1.0, equivalent to a protein concentration of 14 to 95 μg mL^{-1}. Formation of NADH was followed spectrophotometrically at 365 nm[25] using sealed 3.5 mL cuvettes containing 2 mL of reaction mixture under an atmosphere of 1 bar H_2. The detection limits for H_2-dependent NAD^+ reduction activities were 0.15, 0.1, and 0.3 U mg^{-1} of protein for crude extracts, soluble extracts, and purified protein, respectively. H_2 consumption measurements in the presence of defined gas mixtures were done in a reversed Clark-type electrode[49] with a 1.3 mL reaction chamber (without headspace) using different ratios of H_2-, O_2-, and N_2-saturated buffers.

Methyl Viologen-Dependent H_2 Production Assay. Methyl viologen dichloride (MV)-dependent H_2 production was assayed in rubber septum-sealed 7.6 mL vials containing reaction mixtures composed of 1.3 mL of N_2-saturated Tris/HCl buffer (50 mM, pH 8.0), 5 mM MV, 7 mM sodium dithionite (DT), and 1−5 μg of purified SH or CTAB-lysed cells (approximately 150 μg mL^{-1} final protein concentration) under an atmosphere of 1 bar N_2. After incubation for 30 min at 30 °C, the reaction was stopped on ice and aliquots of the gas phase were analyzed by gas chromatography as previously described.[22] The detection limits for MV-dependent H_2 production activities were 0.001 and 0.1 U mg^{-1} of protein for whole-cell extracts and purified protein, respectively.

NADH:BV-Oxidoreductase (Diaphorase) Activity Assay. NADH-dependent reduction of benzyl viologen dichloride (BV) was measured spectrophotometrically at 550 nm ($\varepsilon_{BV,red}$ = 7.8 mM^{-1} cm^{-1}). Rubber-sealed cuvettes contained 2 mL of N_2-saturated Tris/HCl buffer (50 mM, pH 8.0), 0.6 mM NADH, 0.6 mM BV, and either CTAB-lysed cells (15−40 μg mL^{-1} final protein concentration) or 0.8−2.5 μg of purified SH protein. The measurement was done at 30 °C under an atmosphere of 1 bar N_2.

H/D Exchange Measurements. H_2/D^+ isotopic exchange experiments were performed using the setup described in ref 20. The reaction buffer (50 mM Tris/HCl) was prepared with D_2O (99.8 atom % D) and adjusted to an apparent pH of 7.6 (equivalent to a pD of 8.0[50]). Two milliliters of buffer were bubbled with H_2 to saturation in the reaction chamber. Then, 15 nmol NADH and 10 μmol DT were added, and the reaction was started with 2−5 μg of purified SH protein. Formation of HD (m/z = 3) and D_2 (m/z = 4) was followed online by mass spectrometry, and the data were corrected for gas consumption by the mass spectrometer. In a control reaction, formation of D_2 through NADH-dependent D^+ reduction was tested with air-saturated buffer and turned out to be at least 1 order of magnitude lower than H_2-dependent D_2 formation activity via H/D exchange.

Determination of Protein and FMN Concentration. Protein concentrations were determined with the bicinchoninic acid (BCA) kit (Pierce/Thermo Scientific, Rockford, IL, USA) using bovine serum albumin as reference. The flavin mononucleotide concentrations in neutralized trichloroacetic acid extracts of the purified SH variants were analyzed fluorometrically with a Spectramax M4 spectrofluorometer at λ_{ex} = 430 nm and λ_{em} = 526 nm, essentially as described in ref 25 but adapted for a 96-well plate. FMN (Sigma-Aldrich Chemie GmbH, Steinheim, Germany) was used as standard.

SDS-PAGE and Immunological Analysis. Proteins were separated by SDS polyacrylamide gel electrophoresis (SDS-PAGE)[51] and either directly visualized by Coomassie brilliant blue G-250 staining or transferred to a nitrocellulose membrane for immunological detection. Polyclonal rabbit antisera raised against HoxH and HoxY were used for the detection of the SH subunits in dilutions of 1:25000 and 1:5000, respectively. Alkaline phosphate-conjugated to goat anti-rabbit IgG secondary antibody (Dianova, Hamburg, Germany) allowed the visualization the antigen−antibody complexes. The lanes were supplied with either 5 μg of purified protein, 5 μg total protein of the soluble extract, or cell suspension corresponding to an OD_{436} of 0.1.

DOI: 10.1021/bi501347u
Biochemistry 2015, 54, 389−403

UV−Vis Spectroscopy. UV−visble spectra were recorded with a CARY 5000 UV−vis−NIR spectrophotometer (Varian) at 12 °C. A quartz cuvette with an optical path length of 1 cm was filled with 100 μL of protein solution at a concentration of 1 to 1.5 mg mL^{-1}. The UV−vis spectra were normalized to the protein concentration.

FTIR and EPR Spectroscopy. The setup and measurement conditions for FTIR spectroscopy were the same as described in ref 37. Sample concentrations were as follows: SH^{WT}, 0.29 mM; SH^{C39G}, 0.24 mM; SH^{C39S}, 0.3 mM; SH^{C41S}, 0.15 mM; and SH^{W42S}, 0.25 mM. IR difference spectra over the entire 1000−4000 cm^{-1} spectral range were collected with a thin-layer transmission cell with an optical path length of about 5 μm.[52] In this case, concentration of both the SH^{WT} and SH^{W42S} proteins was 0.32 mM. X-band EPR spectra were recorded at 9.3 GHz using a Bruker "EMX Plus" spectrometer equipped with a high-sensitivity Bruker Superhigh-Q-cavity (ER 4122 SHQE). Samples were prepared in quartz tubes with an outer diameter of 4 mm. To avoid cracking the quartz tubes, they were first frozen in cold ethanol (ca. 220 K) and thereafter immediately transferred into a liquid nitrogen storage. For EPR analysis, the samples were placed in an Oxford EPR 900 helium flow cryostat that allows temperature control between 5 and 200 K (Oxford ITC4). The EPR instrument settings are given in the figure legend. When required, baseline corrections were performed by subtracting a background spectrum obtained from a sample containing only a buffer solution under the same experimental conditions.

For spin quantification, the EPR signal of the fully reduced $[2Fe−2S]^+$ cluster (NADH and H_2) at 35 K was used as an internal spin standard (one spin/protein). The sample volume was kept constant for all measurements. When comparing signal intensities between different samples (e.g., from oxidized samples), differences in sample concentration and temperature effects were taken into account.

Reduced samples were prepared anaerobically in a glovebox (filled with 95% (v/v) N_2 and 5% (v/v) H_2) at room temperature by addition of 5 mM NADH (anaerobic solution through Ar bubbling) and subsequent incubation for 30 min under 1 bar H_2. For one sample, SH^{C41S}, 10 mM DTT (anaerobic solution) was added. NADH-reduced samples were prepared anaerobically at room temperature under a 100% (v/v) N_2 atmosphere by addition of 10 mM NADH (anaerobic solution).

Bioinformatics. The amino acid sequences of the HoxY homologous proteins were retrieved from the NCBI protein and UniProt databases. Multiple alignments were performed with ClustalW[53] and refined manually using Jalview 2.7.[54] Structural information and PDBs of HydA from *Desulfovibrio vulgaris* Mirazaki F (1WUJ) and of Nqo6 from *Thermus thermophilus* (3IAM) were retrieved from RCSB Protein Data Base and visualized with PyMOL 1.3. Modeling of the *R. eutropha* HoxY structure was done with SWISS-MODEL (swissmodel.expasy.org) using the above-mentioned structures and *R. eutropha* HoxK (3RGW) as templates. Mutagenesis of *hoxY* was planned with the aid of ApE v1.17 (http://biologylabs.utah.edu/jorgensen/wayned/ape/).

RESULTS

Amino Acid Exchanges in the Iron−Sulfur Cluster-Containing HoxY Subunit. Large parts of the iron−sulfur cluster containing HoxY subunit of the SH belong to a core structure that is also present in small subunits of group 1 [NiFe]-hydrogenases and the Nqo6 subunit of Complex I (Figure 2). This motif comprises at least four cysteine residues embedded in a structure consisting of a 4-stranded parallel β-sheet sandwiched by α-helices (Figure 2A). On the basis of this similarity, we derived a topology model of HoxY (Figure 2B). Four of the cysteine residues (marked in red) are highly conserved and are involved in coordination of the proximal [4Fe−4S] cluster in group 1 [NiFe]-hydrogenases (Figure S1). However, the HoxY subunit carries five additional cysteines (yellow) that are not present in the O_2-sensitive bidirectional hydrogenases of cyanobacteria (Figure S1). To investigate their function, the five supernumerary cysteine residues, C39, C79, C104, C131, and C166, were exchanged by the corresponding amino acids present in the HoxY subunits of cyanobacterial enzymes. Residue C39 was additionally substituted by serine and alanine. For control, each of the conserved cysteine residues, C41, C44, C113, and C179, was exchanged by glycine and serine. Furthermore, the three histidine residues, H12, H99, and H153, were replaced by glutamates, which are present at the corresponding positions in the cyanobacterial hydrogenases (Figures S1 and 2). Finally, the tryptophan residue W42, which seems to be characteristic for O_2-tolerant NAD^+-reducing hydrogenases and might be involved in binding of the FMN-a, was replaced by serine. All exchanges were established in an SH variant carrying a *Strep*-tag II affinity peptide at the N-terminus of the HoxF subunit. The corresponding alleles were introduced into the genome of a *R. eutropha* derivative carrying in-frame deletions in the large subunit genes, *hoxG*, *hoxC*, and *hofG* of the MBH, the regulatory hydrogenase (RH),[55] and the recently discovered Actinobacterial Hydrogenase (AH),[56] respectively. The SH represents, therefore, the only H_2-oxidizing enzyme synthesized in these strains. For simplicity, both the bacterial strains and the SH variants were named according to the corresponding amino acid exchange in HoxY, e.g., SH^{C39G} and SH^{W42S}. An overview of the characterization of all mutant strains and SH variants can be found in Table S3.

Effects of the Amino Acid Exchanges in HoxY on Lithoautotrophic Growth and Catalytic Activity in Cell Extracts. To test the capability of the *hoxY* mutant strains to grow lithoautotrophically, cell suspensions were streaked on mineral agar plates and incubated under an atmosphere of 3% (v/v) H_2, 10% (v/v) CO_2, and various concentrations of O_2 (Table 2 and Figures S2 and S3). Compared to the SH^{WT} control, the SH^{W42S} strain and all mutants carrying exchanges in one of the canonical cysteines, C41, C44, C113, and C179, showed no growth at all. Even in the presence of only 2% (v/v) O_2, no growth was observed (Table 2 and Figure S3). By contrast, strains harboring exchanges in one of the cysteine or histidine residues specific to O_2-tolerant NAD^+-reducing hydrogenases showed wild-type-like growth in the presence of 10% (v/v) O_2 (Table 2 and Figure S2). However, except for SH^{C131V}, all of these strains displayed at least slightly slower growth in the presence of 35% (v/v) O_2. A severe response toward high O_2 concentrations (20 and 35%) was observed for the strains carrying amino acid exchanges C39G, C39A, C104S, H12E, and H153E (Table 2 and Figure S2).

To test whether the growth effects correlate with SH activity, the mutant strains were grown heterotrophically under SH synthesis conditions (see Material and Methods). H_2-driven NAD^+ reduction activities were determined either in permeabilized cells or in soluble cell extracts. Permeabilized cells of strains SH^{C41G}, SH^{C41S}, SH^{C44G}, SH^{C44S}, SH^{C113G}, SH^{C113S}, SH^{C179G}, SH^{C179S}, and SH^{W42S} did not show H_2-oxidizing

DOI: 10.1021/bi501347u
Biochemistry 2015, 54, 389−403

Table 2. SH-Based Lithoautotrophic Growth of Mutant Strains at Increasing O_2 Concentrations[a]

	2% O_2	10% O_2	20% O_2	35% O_2
SH^{C41G}	ø	ø	n.d.	n.d.
SH^{C41S}	ø	ø	n.d.	n.d.
SH^{C44G}	ø	ø	n.d.	n.d.
SH^{C44S}	ø	ø	n.d.	n.d.
SH^{C113G}	ø	ø	n.d.	n.d.
SH^{C113S}	ø	ø	n.d.	n.d.
SH^{C179G}	ø	ø	n.d.	n.d.
SH^{C179S}	ø	ø	n.d.	n.d.
SH^{C39G}	n.d.	++++	++	+
SH^{C39A}	n.d.	++++	+++	++
SH^{C39S}	n.d.	++++	++++	+++
SH^{C79V}	n.d.	++++	++++	+++
SH^{C104S}	n.d.	++++	+++	+
SH^{C131V}	n.d.	++++	++++	++++
SH^{C166V}	n.d.	++++	++++	+++
SH^{H12E}	n.d.	++++	+++	++
SH^{H99E}	n.d.	++++	++++	+++
SH^{H153E}	n.d.	++++	+++	+
SH^{W42S}	ø	ø	n.d.	n.d.

[a]Synchronized strains were plated on mineral agar plates without a carbon source and incubated under an atmosphere of 10% (v/v) CO_2, 3% (v/v) H_2, x% (v/v) O_2, and (87 − x)% (v/v) N_2 for 5 days. Growth behavior of the mutant strains was evaluated in comparison to that of a SH^{WT} strain: ++++, WT-like growth; +++, slightly reduced growth; ++, reduced growth; +, strongly reduced growth; ø, no growth; n.d., not determined. The given results are deduced from at least three independent experiments. Agar plates of one representative experiment are shown in Figures S2 and S3.

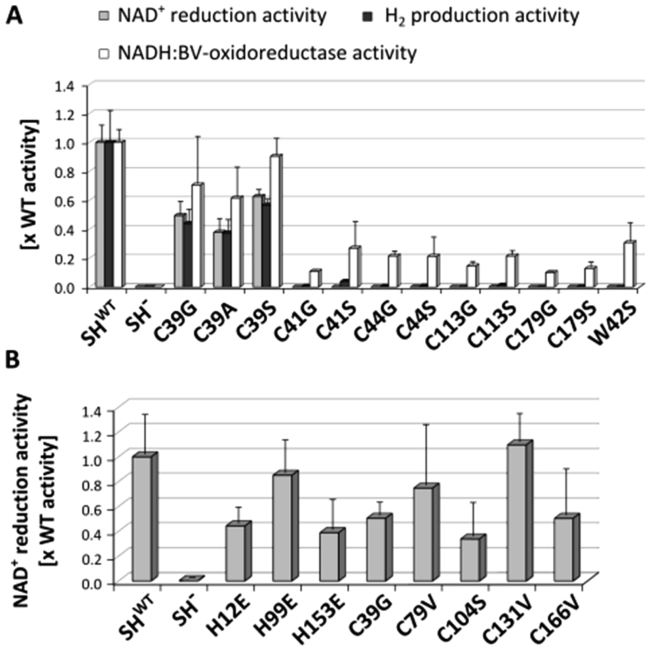

Figure 3. SH-specific activities in crude cell and soluble extracts of the mutant strains. Strains were grown heterotrophically under O_2-limited conditions. H_2-dependent NAD^+ reduction activities in (A) crude extracts or (B) soluble extracts were determined spectrophotometrically. Methly viologen-dependent H_2 production activities and NADH-dependent benzyl viologen reduction activities in panel A were determined by gas chromatography and spectrophotometrically, respectively. Crude extracts were prepared by cell lyses with CTAB directly before the activity measurements. An amount of 38−190 μg of total protein mL^{-1} was used in the assays. Data are the mean and standard derivation of three independent experiments. WT activities were (A) 2.03 ± 0.23 μmol NADH min^{-1} mg^{-1} protein, 0.35 ± 0.07 μmol H_2 min^{-1} mg^{-1} protein, and 0.46 ± 0.04 μmol BV min^{-1} mg^{-1} protein and (B) 3.7 ± 1.2 μmol NADH min^{-1} mg^{-1} total protein.

activity, which is entirely consistent with the growth phenotype (Figure 3A). Interestingly, strain SH^{C41S} was still capable in methyl viologen (MV)-mediated H_2 production at 5% of the wild-type level. The NADH-mediated benzyl viologen reduction activity (NADH:acceptor oxidoreductase activity) of the aforementioned strains was decreased to 10−27% of the wild-type level (Figure 3A), indicating a destabilization of the diaphorase module as a result of the amino acid substitutions in the hydrogenase moiety. Considerably higher NADH:acceptor oxidoreductase activities (60−90% of wild-type activity) were observed for strains SH^{C39G}, SH^{C39A}, and SH^{C39S}. These strains showed H_2-dependent NAD^+ reduction and MV-driven H_2 production activities of approximately 50% of that the wild-type levels (Figure 3A). Soluble cell extracts were prepared from those strains that showed retarded lithoautotrophic growth. The corresponding H_2-dependent NAD^+ reduction activity measurements revealed that strains SH^{H12E}, SH^{C79V}, and SH^{C131V} preserved 75−100% of wild-type activity, whereas strains SH^{H12E}, SH^{H153E}, SH^{C39G}, SH^{C104S}, and SH^{C166V} contained activity that was 50% or less than that of SH^{WT} (Figure 3B).

The diminished diaphorase activity in most of the mutant strains already indicated instability of the SH variants. To test whether the growth defects were just a result of protein instability, the soluble cell extracts were analyzed immunologically with specific antibodies against the subunits of the hydrogenase module, HoxY and HoxH. As shown in Figure S4, both subunits were still detectable in all mutant strains except for the SH^- control. The amount of the hydrogenase large subunit HoxH was not significantly altered in any of the mutant strains. The amount of the HoxY subunit was, however, decreased in strains carrying the exchanges H12E, H153E, C41G, C113G, C113S, C179G, and C179S, indicating HoxY instability, at least to some extent.

Purification of Selected SH Variants. To obtain detailed insight into the stability, catalytic activity, and spectroscopic properties of the SH holoprotein, the variants $SH^{C39G/A/S}$, $SH^{C41G/S}$, SH^{C44S}, SH^{C113S}, SH^{C179S}, and SH^{W42S}, which possess amino acid exchanges directly at or close to the proximal Fe−S cluster, were purified from heterotrophically grown cells by affinity chromatography. Preparations of $SH^{C39G/A/S}$ and SH^{W42S} yielded wild-type-like amounts (1−2 mg of purified SH from 1 g (wet weight) of cells) and showed a normal subunit stoichiometry (Figure 4). By contrast, the SH variants carrying exchanges of the canonical cysteine residues (C41, C44, C113, and C179) could be purified only in low amounts corresponding to approximately 25% of the wild-type yield. While the subunit stoichiometry of the SH^{C41S} variant seemed to be intact, the SH^{C44S}, SH^{C113S}, SH^{C179S}, and SH^{C41G} complexes carried considerably lower amounts of the hydrogenase module subunits HoxH and HoxY (Figure 4). Notably, these preparations also contained a truncated version of the subunit HoxU (designated HoxU*, Figure 4). This observation has been made earlier for the isolated SH diaphorase module, HoxFU, and has been related to an as yet unidentified protein modification.[27] The fact that the HoxU truncation obviously

DOI: 10.1021/bi501347u
Biochemistry 2015, 54, 389−403

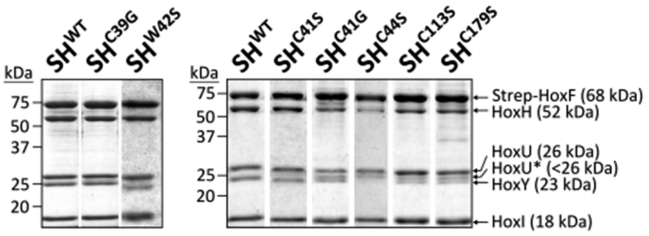

Figure 4. Purified SH variants and SH^{WT}. Selected SH variants were purified by affinity chromatography via a *Strep*-Tag II peptide fused to HoxF. Equivalents of 5 μg of protein were subjected to a 15% SDS-PAGE and visualized with Coomassie brilliant blue staining.

correlates with substoichiometric presence of the hydrogenase module suggests partial degradation.

Next, we measured the H_2-driven NAD^+ reduction activities of the purified proteins. The assays were prepared with 1 mM DTT and 1 μM FMN; both components have been shown to enhance and stabilize the catalytic activity of the SH (Figure S5).[22] Variants SH^{C39S} and SH^{C39A} displayed 83 and 50%, respectively, of the wild-type activity (Table 3), which is in agreement with the data obtained with crude extracts. Only 31% of wild-type activity was determined for the SH^{C39G} variant, which is considerably lower than the activity in the crude extract and suggests that the activity suffers as a result of the purification procedure (Table 3). The SH^{W42S} protein displayed neither NAD^+ reduction activity nor MV-dependent H_2 production (Table 3 and Table S4). The NADH-dependent BV reduction activity, however, was unchanged compared to that of the SH^{WT} complex (Table S4), indicating that the inability in H_2 cycling was solely due to an inactive hydrogenase module.

Table 3. NAD^+ Reduction and H_2 Production Activities of Purified SH Variants

	NAD^+ reduction activity[a] (U mg^{-1})	MV-dependent H_2 production activity[a] (U mg^{-1})
SH^{WT}	115.9 ± 17.4	11.2 ± 2.0
SH^{C39G}	36.3 ± 2.7	2.0 ± 0.9
SH^{C39A}	57.1 ± 4.9	3.3 ± 0.2
SH^{C39S}	96.0 ± 8.0	n.d.
SH^{C41S}	8.7 ± 5.9	1.1 ± 0.3
SH^{C44S}	0.4 ± 0.1	<0.1
SH^{C113S}	0.9 ± 0.1	<0.1
SH^{C179S}	0.6 ± 0.5	<0.1
SH^{C41G}	0.9 ± 0.7	0.2 ± 0.1
SH^{W42S}	<0.3	<0.1

[a]NAD^+ reduction activities were measured photometrically in the presence of 1 mM DTT and 1 μM FMN. About 0.7 μg of SH^{WT}/$SH^{C39G/A/S}$ complex and 7−15 μg of the further SH variants were used in the assay. MV-dependent H_2 production was assayed by gas chromatography. About 1.2 μg of the SH^{WT}/$SH^{C39G/A/S}$ complex and 10−20 μg of the further SH variants were used in the assay. An amount of 1 U corresponds to the conversion of 1 μmol of substrate/product per min. The given values represent the mean and standard deviation of at least two independent preparations of each SH variant. n.d., not determined.

As expected, SH proteins carrying exchanges in the canonical cysteines C41, C44, C113, and C179 showed no significant H_2-driven NAD^+ reduction and MV-dependent H_2 production activities under standard reaction conditions. However, the SH^{C41S} variant exhibited interesting catalytic behavior. At high protein concentration and after an unusually long lag phase of 30 min or more, the H_2-driven NAD^+ reduction activity reached 7.5%, on average, of the wild-type level (Figure 5 and Table 3). In comparison to all other SH derivatives, however, the SH^{C41S} variant showed the largest variance in activity, which is clearly demonstrated in Table S5 on the basis of two independent preparations. The presence of FMN in the assay had a positive effect on the activity (Table S5), as was previously observed for the wild-type protein.[22,39] Both the length of the lag phase and the maximal catalytic activity depended on the enzyme concentration in the assay (Figure 5), suggesting a beneficial synergistic interaction of the individual SH molecules in the solution. Most notably, in contrast to SH^{WT}, the addition of reductant (DTT, Tris(2-chlorethyl)-phosphate (TCEP), or β-mercaptoethanol) was mandatory for the development of H_2-driven NAD^+ reduction activity by the SH^{C41S} protein (Figure 5B and Table S5). In spite of the comparatively high statistical error, the highest activity of 13.2 U mg^{-1} of protein (10% of wild-type activity) was observed in the presence of both DTT and FMN. Consistently, the MV-dependent H_2 production activity also reached approximately 10% of the wild-type level (Table 3).

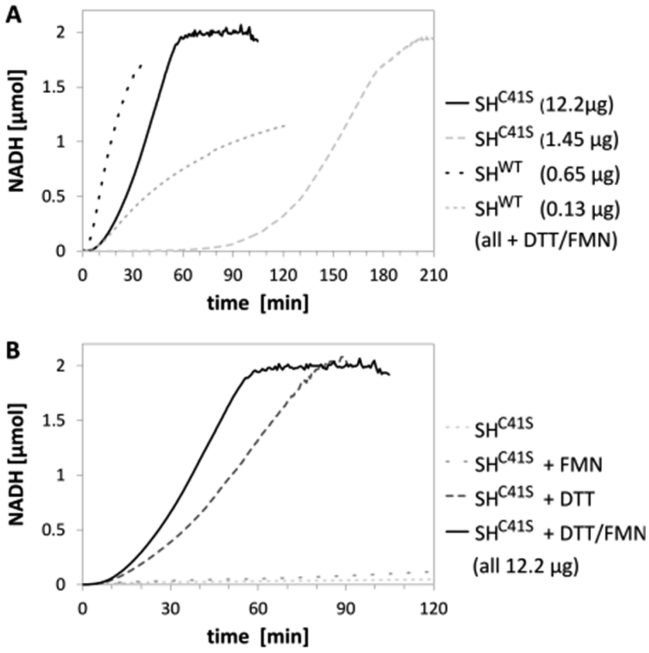

Figure 5. H_2-dependent NAD^+ reduction kinetics of SH^{C41S} measured in the presence of FMN and/or DTT. The assays were performed in H_2-saturated 50 mM Tris/HCl buffer, pH 8.0, with 1 mM NAD^+ at 30 °C. When indicated, the assays also contained 1 mM DTT and/or 1 μM FMN. The reactions were started at t = 0 min by the addition of the indicated amounts of purified enzyme. (A) Kinetics of NADH formation for different amounts of SH^{C41S} and SH^{WT}. (B) Influence of the additives (FMN, DTT) on the kinetics of SH^{C41S}. The graphs depict representative examples of repeated measurements. Activities of two independent SH^{C41S} preparations under various conditions are presented in Table S5.

SH Proteins Carrying Exchanges in C39 Show Enhanced Oxygen Sensitivity. The purified variants $SH^{C39G/A/S}$, which showed considerable catalytic activity, were tested for their ability to catalyze H_2-driven NAD^+ reduction in the presence of O_2. Activities were determined in the presence of H_2 either in the absence or presence of 585 μM O_2 (50% O_2

DOI: 10.1021/bi501347u
Biochemistry 2015, 54, 389−403

saturation in the reaction assay). The H_2-driven NAD^+-reduction activity by the SH^{WT} enzyme slightly decreased in the presence O_2, which is consistent with earlier observations (Table 4 and Figure S6).[22,33] The SH^{C39G}, SH^{C39A}, and SH^{C39S} variants showed 21, 46, and 51% of the wild-type activity, respectively, in the absence of O_2. However, unlike the SH^{WT} enzyme, all three variants lost 20−34% of their initial activity in the presence of O_2 (Table 4). Furthermore, while the H_2 gas was completely consumed in the absence of O_2, and for the wild-type enzyme even in the presence of O_2, the $SH^{C39G/A/S}$ proteins were not capable of oxidizing the provided H_2 completely in the presence of O_2, suggesting continuous enzyme inactivation during catalysis (Figure S6).

Table 4. Impact of O_2 on the H_2-Dependent NAD^+ Reduction Activities of Purified SH^{WT} and $SH^{C39G/A/S}$ Proteins

SH variant	NAD^+ reduction activity in the absence of O_2[a] (U mg^{-1} SH)	NAD^+ reduction activity in the presence of O_2[a] (U mg^{-1} SH)	ratio of activity in the presence of O_2 /activity in the absence of O_2
SH^{WT}	117 ± 12	111 ± 11	0.95
SH^{C39G}	24 ± 1	19 ± 4	0.80
SH^{C39A}	54 ± 4	36 ± 1	0.66
SH^{C39S}	60 ± 3	46 ± 5	0.76

[a]All activities were measured with an inverted Clark-type electrode setup. The assay was performed in a 1:1 mixture of N_2/H_2-saturated buffer (absence of O_2) or of O_2/H_2-saturated buffer (presence of O_2, 585 μM O_2) at 30 °C. In all experiments, 1 mM NAD^+, 1 mM DTT, 1 μM FMN, and about 75 mU of enzyme were applied. One unit corresponds to the consumption of 1 μmol H_2 min^{-1}. The given values represent the mean and standard derivation of at least three measurements.

Spectroscopic Characterization of Selected SH Variants by EPR Spectroscopy. The iron−sulfur cluster in HoxY from *R. eutropha* appears to be silent in electron paramagnetic resonance (EPR) spectroscopy measurements.[28,38] To test whether the amino acid substitutions in close vicinity of the proximal [4Fe−4S] cluster altered the spectroscopic behavior of the cofactor, the SH^{C39G}, SH^{C39S}, SH^{C41S}, and SH^{W42S} proteins were subjected to EPR and UV−visible absorption spectroscopy. The UV−visible absorption spectra of the SH variants did not reveal any obvious differences to the SH^{WT} spectrum in the range between 320 and 500 nm (Figure S7). However, the strong absorptions of one [2Fe−2S] cluster, three [4Fe−4S] centers, and two FMN molecules, which are proposed to be additional constituents of the SH, leaves an interpretation that is challenging to make.

EPR measurements were performed with the as-isolated, oxidized proteins as well as with protein samples reduced either with NADH or with both H_2 and NADH (Figure 6). The EPR spectra of the oxidized proteins did not show major differences. All of them contained a signal that can be attributed to a $[3Fe-4S]^+$ cluster. However, spin quantification revealed that this signal corresponds only to approximately 10% of the molecules (Figure 6B), indicating partial oxidative damage of one or more [4Fe−4S] clusters.[38] In the case of SH^{C41S}, even 20% of the protein molecules contained this signal. Furthermore, the oxidized SH^{WT}, SH^{C39G}, and SH^{C39S} proteins showed traces (~3%) of a signal derived from the active site attributable to the Ni_r−B state characterized by a hydroxy ligand between the Ni(III) and Fe(II) ion.[57]

Upon reduction with either NADH alone or with NADH and H_2, the Ni_r−B-related EPR signal disappeared, suggesting a reductive removal of the OH^- species. The Ni_r−B signal was entirely absent in the SH^{C41S} and SH^{W42S} variants (Figure 6). Because of the low abundance of both the Ni_r−B- and $[3Fe-4S]^+$-related EPR signals, the relevance of these redox species for the function of native SH is questionable.

Upon reduction with H_2 and NADH, no major differences were observable between the five SH variants. The spectra were dominated by signals attributable to one $[2Fe-2S]^+$ cluster and reduced [4Fe−4S] cluster species. Spin quantification is in accordance with only one $[4Fe-4S]^+$ cluster in 60% of the SH molecules (Figure 6), leaving it unclear as to whether the EPR signal is derived from only one or several partially reduced [4Fe−4S] clusters. However, the data suggest that the majority of the presumed [4Fe−4S] clusters in the SH is EPR-silent or have a lower reduction potential than that achieved through incubation with NADH and H_2. Notably, the $[4Fe-4S]^+$ signal intensity in the SH^{C41S} and SH^{W42S} variants is only 45%.

The most striking differences were observed in the spectra of the NADH-reduced enzymes (Figure 6). This rather mild reductive treatment led to the accumulation of the Ni_a−C state, which has been observed previously to be most intense at a redox potential of about −300 mV.[41] Previous results obtained with different [NiFe]-hydrogenases in the Ni_a−C state revealed a hydride present in the bridge between Ni(III) and Fe(II) in the catalytic center.[58,59] Analysis of the EPR spectra revealed that approximately 35% of the SH^{WT} protein resided in the Ni_a−C state. Ten times less Ni_a−C signal was observed for the SH^{C41S} variant, whereas the signal of the SH^{W42S} protein was below the detection limit (<2%) (Figure 6B). Quantitative reduction of the [2Fe−2S] cluster species upon NADH treatment and the presence of a signal corresponding to a FMN-derived semiquinone radical indicates that the diaphorase module is still functional in all of the SH variants. These data are fully consistent with the activity measurements depicted in Table 3.

Investigation of the [NiFe] Active Site by IR Spectroscopy. Fourier-transform infrared (FTIR) spectroscopy probes for the three diatomic iron ligands, one carbonyl group and two cyanides, bound to the active site iron. The specific vibrational spectroscopic pattern of these ligands is related to the redox state composition of the catalytic center.[38,59] The SH^{C39G} and SH^{C39S} variants did not show major differences compared to the SH^{WT} protein (Figure S8). The as-isolated, oxidized protein samples displayed a major CO-derived absorption band at 1957 cm^{-1} and four bands with lower intensity between 2068 and 2099 cm^{-1}, which are assigned to CN stretching vibrations. This is the typical band pattern usually observed for the as-isolated SH protein.[42,60,61] Reduction of the protein samples with NADH and H_2 revealed a more complex band pattern, with five absorptions at 1961, 1957, 1946, 1922, and 1913 cm^{-1} in the CO region and four additional absorptions at 2052, 2068, 2080, and 2090 cm^{-1} in the CN stretching region (Figure 7). This band pattern represents a mixture of the five different reduced states, Ni_a−C, Ni−SR, Ni−SR′, Ni−SR″, and Ni−SR2, with partially overlapping bands, which have already been described for the reduced SH protein both *in vitro* and *in vivo*.[37,42] The intensity of the absorption band related to the Ni_a−C species with CO and CN stretchings at 1962 and 2079/2089 cm^{-1}, respectively, is compatible with the quantification derived from the EPR analysis (~30%).

DOI: 10.1021/bi501347u
Biochemistry 2015, 54, 389−403

A

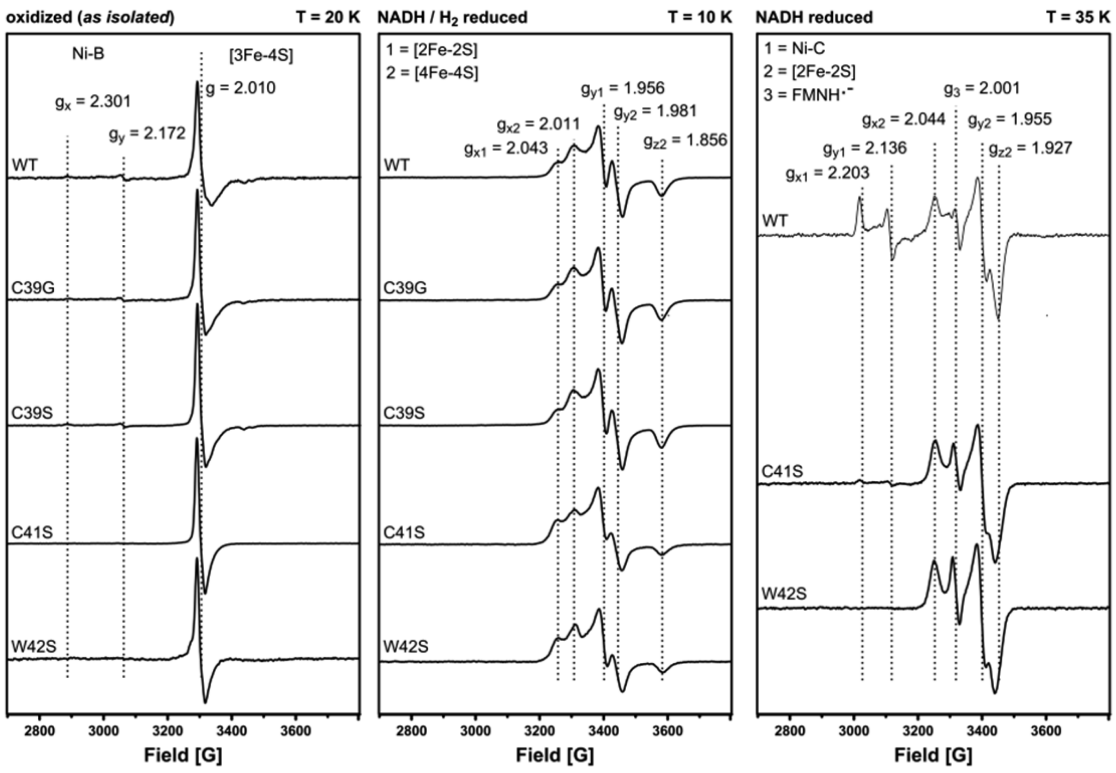

B

	oxidized (*as isolated*)		NADH/H_2-reduced		NADH-reduced[2]	
	Ni-B	[3Fe4S]	[2Fe2S]	[4Fe4S][1]	[2Fe2S]	Ni-C
SH^{WT}	3 %	10 %	100 %	60 %	54 %	35 %
SH^{C39G}	3 %	12 %	100 %	60 %	n.d.	n.d.
SH^{C39S}	3 %	12 %	100 %	60 %	n.d.	n.d.
SH^{C41S}	< 2 %	19 %	100 %	45 %	52 %	4 %
SH^{W42S}	< 2 %	11 %	100 %	45 %	58 %	< 2 %

Figure 6. EPR spectra of the SH^{C39G}, SH^{C39S}, SH^{C41S}, and SH^{W42S} variants in comparison with SH^{WT}. (A) Spectra of the as-isolated, air-oxidized samples (~0.3 mM of SH) were recorded at 20 K (left panel). Prior to reduction, oxygen was removed by applying 10 vacuum/Ar-purging cycles to the protein samples. For reduction with NADH and H_2, NADH was first added to the protein solution (c_{final} = 5 mM). The NADH-treated samples were then incubated with H_2 for 30 min at room temperature. Spectra recorded for reduced SH at 35 and 20 K showed only [2Fe−2S] cluster signals (not shown). The corresponding spectra recorded at 10 K showed both [2Fe−2S] and [4Fe−4S] cluster signals (middle panel). The spectrum of an additionally prepared NADH/H_2/DTT-reduced SH^{C41S} sample (with c_{final} = 10 mM DTT) did not differ from those of the standard NADH/H_2-reduced sample of this SH variant (data not shown). Spectra of samples reduced solely with NADH (c_{final} = 10 mM) were recorded at 35 K and showed signals of both the [2Fe−2S] cluster and the active site in the paramagnetic Ni_a−C state (right panel). Assignment of the signals was based on the characteristic g values as indicated in the spectra. (B) Quantification of the integrated signal intensities (see Material and Methods). The error margin of the given values is ca. 2%. The lack of an obvious signal is referred to as <2% (detection limit).[1] Signal intensities of the [4Fe−4S] cluster were derived from the EPR spectra recorded at 10 K.[2] The signal at g_x = 2.01 arose from a semiquinone radical; n.d., not determined. Experimental parameters: microwave frequency, 9.306 GHz; modulation frequency, 100 kHz; modulation amplitude, 10 G; and microwave power, as-isolated samples: 0.25 mW, 6 min accumulation time, NADH-reduced samples: 1 mW, 3 min accumulation time, NADH/H_2-reduced samples: 1 mW and 6 min accumulation time.

The FTIR spectrum of the as-isolated SH^{C41S} protein also resembled that of SH^{WT} except that the high-frequency CN^- absorptions (2099 and 2089 cm^{-1} in the SH^{WT} spectrum) are slightly shifted by 1−2 cm^{-1} to lower wavenumbers (Figure 7). However, only minor amounts of the SH^{C41S} molecules could be reduced, as demonstrated by the occurrence of only weak absorptions reflecting the reduced Ni-SR, Ni-SR′, and Ni-SR″ species observed at 1946, 1922, and 1913 cm^{-1} (CO stretching vibrations), respectively. In contrast to SH^{WT}, Ni_a−C-related bands could be barely assigned in the spectrum of the protein treated only with NADH (Figure 7). These observations are in good agreement with the low catalytic activity (Table 3) and the substoichiometric Ni_a−C-related EPR signal (Figure 6) of the NADH-reduced SH^{C41S} protein.

The SH^{W42S} protein displayed a completely different spectral pattern than that of the SH^{WT} protein (Figure 7). Compared to SH^{WT}, the CO-related band at 1957 cm^{-1} in the as-isolated protein was broadened and had a considerably lower intensity. Instead, an absorption at 1938 cm^{-1}, which was not present in native SH, showed the highest intensity. Also, the CN^-

DOI: 10.1021/bi501347u
Biochemistry 2015, 54, 389−403

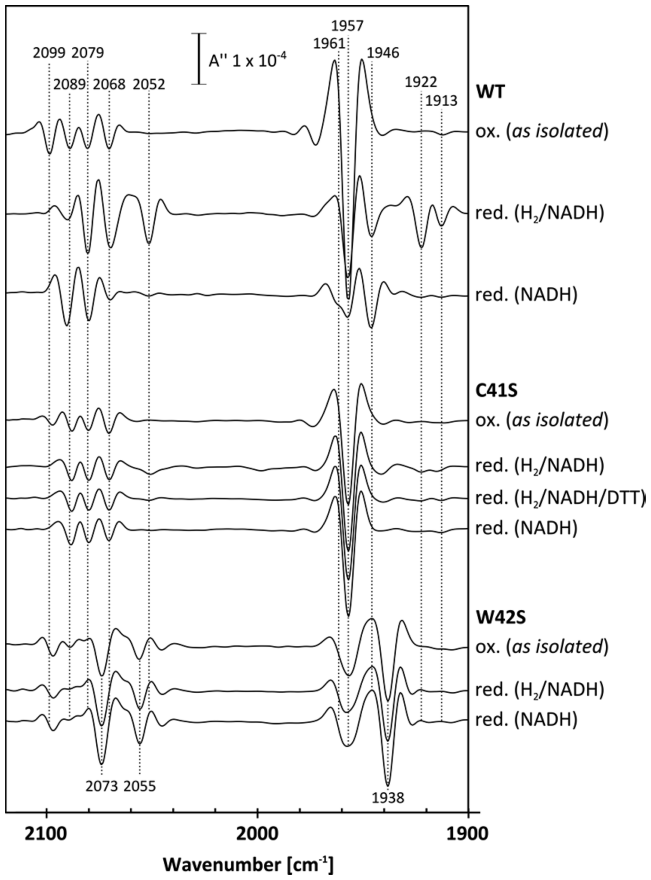

Figure 7. FTIR spectra of the SH^{WT}, SH^{C41S}, and SH^{W42S} complexes. Spectra (second derivative) of the as-isolated, air-oxidized samples were compared to spectra of NADH- and NADH/H_2-reduced samples (protein concentration: 0.3 mM). For NADH/H_2 reduction, NADH (c_{final} = 5 mM) was added to the protein solution, and the samples were incubated with H_2 for 30 min. The SH^{C41S} sample reduced with NADH, H_2, and DTT additionally contained 10 mM DTT. For NADH reduction, NADH was added to a final concentration of 10 mM. Absorption bands corresponding to individual redox states (see text) are indicated by dotted lines. The shoulder at 1961 cm^{-1} in the spectrum of the NADH-reduced sample (trace 3) is indicative of the Ni_a−C state. In the presence of NADH and H_2 (trace 2), this state is depopulated in favor of more reduced species. Nonetheless, the asymmetry of the second-derivative signal at 1957 cm^{-1} in trace 2 (the intensity decrease at the high-frequency edge reflects a decline of the curvature, indicating a local maximum) indicates minor amounts of the Ni_a−C state.

stretching region displayed structural heterogeneity. The bands usually present in the as isolated wild-type spectrum generally appeared with low intensity and partially overlapped with two new major stretchings at 2073 and 2055 cm^{-1}. The band positions did not change upon reductive treatment. This indicates that the [NiFe] center in the SH^{W42S} protein is redox-inactive, which is entirely in line with the activity measurements (Table 3). To check whether the W42S exchange affects the protein backbone structure, we analyzed the IR difference spectrum of SH^{WT} and SH^{W42S} (Figure S9). Indeed, distinct changes of amide I stretching vibrations were observed, indicating local modifications of the protein backbone structure. Thus, the W42S exchange affects the protein folding of the HoxY subunit, which, in turn, might alter the protein environment of the diatomic active site ligands in the HoxH subunit.

H/D-Exchange Activity and FMN Content of the SH^{W42S} Variant. The activity measurements and the spectroscopic characterization of the SH^{W42S} protein suggest that the function of the [NiFe] active site is severely damaged. The integrity of the active site was further investigated by determining H_2/D^+ isotopic exchange activity that does not rely on electron transfer to an iron−sulfur cluster. Even under conditions that facilitate reductive reactivation, i.e., in the presence of 7.5 μM NADH and 5 mM sodium dithionite, the H_2-dependent HD and D_2 formation rates of SH^{W42S} were negligible compared to those for the wild-type enzyme (Table S4). As aromatic amino acids are often involved in the stabilization of flavins,[62−65] we determined the FMN content in the SH^{W42S} protein. However, both the SH^{W42S} and SH^{WT} proteins contained the same amount of 1.0−1.4 FMN per molecule (Table S4). Therefore, there is no indication of the involvement of the tryptophan residue in the coordination of the FMN-a cofactor.

DISCUSSION

In contrast to cyanobacterial $NAD(P)^+$-dependent hydrogenases, the SH of *R. eutropha* catalyzes H_2 oxidation in the presence of O_2.[31,33] It has been shown in a number of recent studies that the unusual structure and coordination of the [4Fe−3S] cluster, which is located in the proximal position relative to the active site, plays a key role in the O_2 tolerance of certain membrane-bound [NiFe]-hydrogenases.[11−14,20] In this study, we investigated the function of the conserved cysteine residues, C41, C44, C113, and C179, that are likely involved in coordination of the corresponding [4Fe−4S] cluster in the SH. Furthermore, we exchanged residues (H12, C39, W42, C79, H99, C104, C131, H153, and C166) that are present only in the HoxY subunits of putatively O_2-tolerant SH enzymes from various microbes.

As expected, our data revealed that the stability of the SH protein complex, and hence its catalytic function, crucially depends on the four canonical cysteine residues, C41, C44, C113, and C179, which further supports their role in coordination of the proposed [4Fe−4S] cluster in the HoxY subunit. Among the corresponding purified SH derivatives, however, the SH^{C41S} variant showed the highest stability in terms of subunit stoichiometry. In contrast to the derivatives carrying exchanges of C44, C113, and C179, which were catalytically inactive, the SH^{C41S} protein exhibited up to 10% of the wild-type H_2-oxidizing activity. In contrast to the SH^{WT} protein, however, H_2-mediated NAD^+ reduction activity by SH^{C41S} was reached only by reductive reactivation under prolonged incubation with DTT. Oxidized SH generally requires reductive reactivation afforded by electrons that are provided by reverse electron flow. Under native conditions, these electrons are derived from NADH.[25] Therefore, NADH produced from a few catalytically active SH molecules can serve as a trigger to reactivate the still oxidized SH proteins in the reaction assay, which can also be interpreted as intermolecular electron transfer between individual SH molecules in solution, facilitating reductive reactivation. This leads, consequently, to an inverse correlation between the length of the lag phase of the NAD^+ reduction kinetics and the protein concentration, a behavior that is very pronounced in the case of the SH^{C41S} protein (Figure 5). The C41S exchange in the HoxY subunit apparently modifies the redox properties of either the [NiFe] catalytic center or the proximal [4Fe−4S] cluster. This may explain the inactivity of most of the SH^{C41S} molecules and the

DOI: 10.1021/bi501347u
Biochemistry 2015, 54, 389−403

necessity to reductively reactivate the remaining enzyme population with DTT. The hypothesis that the C41S exchange also seriously affects the redox properties of the catalytic center is supported by the observation that only a fraction of the SH molecules can be reduced, as determined both with IR and EPR spectroscopy.

Remarkably, all amino acid exchanges presented in this study did not alter the EPR signals related to Fe−S clusters in the enzyme. Assuming the presence of a [4Fe−4S] cluster in HoxY,[28] this is a quite unexpected result, which is in contrast with the observations for the closely related NAD^+-reducing [NiFe]-hydrogenase of *Rhodococcus opacus* MR11. Both enzymes show high sequence identity,[66] but EPR signals indicative of a $[4Fe−4S]^+$ cluster in the hydrogenase module have been observed only for the *R. opacus* SH. This cluster has been described to be highly susceptible toward oxidation that led to an irreversible conversion into a damaged [3Fe−4S] cluster.[26,67]

In the as-isolated protein samples of the *R. eutropha* SH, we observed substoichiometric EPR signals attributable to a $[3Fe−4S]^+$ cluster species (in approximately 10% of the protein) and only traces of Ni_r−B-related EPR signals (approximately 2%). In the SH^{C41S} variant, approximately 20% of the protein molecules showed the $[3Fe−4S]^+$ signal. This increase might be related to oxidative damage of the putative [4Fe−4S] cluster in HoxY as a result of destabilization caused by the absence of ligand Cys41. However, a concomitant increase of the Ni_r−B signal was not observed. At present, the origin of $[3Fe−4S]^+$ signal and its relevance for the catalytic function of the *R. eutropha* SH remain unclear.

Interestingly, while the nature and intensity of EPR signals related to reduced iron−sulfur clusters were quite similar among all SH variants, the FTIR data of some mutant proteins indicated severe changes (damage) of the active site. Approximately 60% of the SH^{WT} and SH^{C41S} molecules as well as 45% of the SH^{W42S} proteins showed EPR signals corresponding to one stoichiometrically reduced [4Fe−4S] cluster. Thus, the [4Fe−4S] signal is unlikely to be related to the proximal iron−sulfur cluster in HoxY.

As outlined above, the O_2 tolerance of certain membrane-bound [NiFe]-hydrogenases is related to the unusual coordination of the proximal [4Fe−3S] cluster by six cysteine residues. The removal of the two supernumerary cysteines rendered theses enzymes O_2-sensitive.[14,15] The systematic exchange of cysteine and histidine residues potentially involved in coordination of the [4Fe−4S] cluster in HoxY revealed that cysteine C39 has little effect on the O_2 tolerance of the SH. *R. eutropha* cells carrying the $SH^{C39G/A/S}$ variants showed increased O_2 sensitivity during growth on H_2 and CO_2, which was, however, visible only at an O_2 concentration of 20% for the SH^{C39G} protein. In case of the $SH^{C39A/S}$ proteins, effects were visible only at the nonphysiological concentration of 35% O_2. This is in marked contrast to the observations for the *R. eutropha* strain harboring the O_2-sensitive MBH, which showed retarded lithoautotrophic growth already at 2% (v/v) O_2.[14] A more pronounced effect was observed *in vitro*, particularly for the purified SH^{C39G} protein. The H_2-dependent NAD^+ reduction activities of the $SH^{C39G/A/S}$ variants were reduced to 66−80% in the presence of 50% O_2, whereas the activity of the SH^{WT} protein did not suffer significantly from such an O_2 concentration.

To assess the localization of Cys39 in relation to the proposed [4Fe−4S] cluster, we compared HoxY with the crystal structure of the oxygen-sensitive standard hydrogenase from *Desulfovibrio vulgaris* Miyasaki F,[68] which possesses an alanine residue at the position equivalent to Cys39 in HoxY. The alanine appears to be too distant for cluster coordination (8.0 Å between C_β and Fe, Figure 8). However, the presence of three glycine residues in the corresponding region of the SH protein, one of them located between Cys39 and Cys41 (Figures S1), suggests a rather flexible structure that might allow close contact of Cys39 to the [4Fe−4S] cluster in the case of HoxY. The observation of residual SH activity in the absence of the canonical Cys41 residue indicates that its functional role in coordinating the [4Fe−4S] cluster in HoxY might be partially taken over by the nearby Cys39. Without further structural or spectroscopic information, however, no clear decision can be made as to whether Cys39 is directly involved in [4Fe−4S] cluster coordination or acts just as modulator of, e.g., the redox potential of the cofactor.

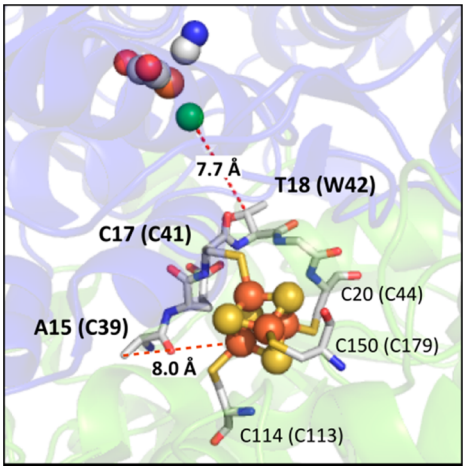

Figure 8. Putative positions of the amino acid residues investigated in this study demonstrated on the basis of the crystal structure of the *Desulfovibrio vulgaris* Miyazaki F hydrogenase (WUJ1). Atoms of the [NiFe] active site and the (proximal) [4Fe−4S] cluster are shown as spheres. Relevant amino acids of the small hydrogenase subunit are displayed in stick representation and labeled according to their type and position in the *D. vulgaris* protein and in *R. eutropha* HoxY (in parenthesis). The large and small hydrogenase subunits (cartoon representation) are colored in blue and green, respectively. The distances between the C_β of the threonine T18 and the active site Ni as well as between C_β of the alanine A15 and the closest iron of the FeS cluster were determined from the crystal structure using PyMOL 1.3.

Another so far unexplained observation for SH-type hydrogenases is the missing of EPR signals related to Ni(III) species of the active site in the oxidized protein samples and signals from most of the proposed [4Fe−4S] clusters in the reduced enzyme. At positive potentials, typical for air-saturated protein solution (>+200 mV), the appearance of Ni(III) with spin $^1/_2$ is expected. Also, the high-frequency CO and CN stretching bands observed by IR spectroscopy in oxidized enzyme samples suggest Ni(III), and they have been therefore assigned to the so-called Ni_r−B-like state.[37,69] Consistent with previous observations, our EPR analyses revealed only 3% Ni(III) signal corresponding to the Ni_r−B state. The absence of stoichiometric, EPR-detectable Ni−B signals appears to be an intrinsic feature of both O_2-sensitive and -tolerant NAD^+-reducing hydrogenases.[38] One possible explanation would be a

DOI: 10.1021/bi501347u
Biochemistry 2015, 54, 389−403

strong magnetic coupling of Ni(III) with the spin of a supposed high-potential iron−sulfur cluster in the HoxY subunit, leading to an overall $S = 0$ spin state. Magnetic coupling between the active site and the proximal [4Fe−3S] cluster has been observed in the *R. eutropha* MBH and related hydrogenases. However, the coupling leads only to a splitting or broadening of the EPR signals, but it is too weak for a complete disappearance of the signals derived from the (super)oxidized cofactors.[16−18]

Furthermore, compared to the substitutions of the supernumerary cysteines coordinating the [4Fe−3S] cluster in O_2-tolerant membrane-bound enzymes, none of the amino acid exchanges in HoxY had a similarly clear effect on O_2 tolerance and spectroscopic properties of the holo-enzyme. Therefore, such a cofactor is unlikely to be present in the SH enzyme, and the reason for the absence of quantitative signals related to Ni(III) is still unclear. There is either another paramagnetic center that couples with the oxidized active site or the active site nickel remains in the Ni(II) state upon oxidation of the enzyme.

Another important result of our study is the observation that tryptophan W42, which is located in direct proximity to the potential [4Fe−4S] cluster and at the interface to the large subunit (Figure 8), is essential for the hydrogenase activity of the SH. The SH^{W42S} variant could be purified in wild-type amounts, and it showed normal NADH-dependent benzyl viologen reduction activity. IR analysis suggests the presence of the [NiFe] catalytic center including cyanide and carbonyl ligands. However, the absorptions of the iron-bound diatomic ligands were detected at unusual band positions. The lack of any hydrogenase activity is consistent with the observation that the IR spectrum did not change at all upon reduction of the as isolated SH^{W42S} protein with either NADH or NADH/H_2. The prominent band at 1938 cm^{-1} in the CO stretching region would be consistent with the presence of the oxidized Ni-Ox2 state that has been reported only for the isolated, but unstable, HoxHY module of the SH.[28] The major CN stretching bands at 2073 and 2055 cm^{-1} of the SH^{W42S} protein, however, could not be assigned to a known oxidized species of the WT. IR difference spectroscopy suggests a partially different folding in the HoxY subunit of the SH^{W42S} protein when compared to that in SH^{WT}. This might also affect the diatomic ligands of the catalytic center, which would be in line with the redox-insensitive spectroscopic manifold observed for the SH^{W42S} protein. We conclude that the W42S exchange, possibly in combination with the concomitant presence of O_2, leads to an irreversible modification of the active site, which prevents catalytic activity. The potential role of O_2 in the inactivation of the SH^{W42S} protein, however, remains to be elucidated.

According to the structure of the *D. vulgaris* hydrogenase, the aromatic side chain of W42 is positioned between the [4Fe−4S] cluster and the catalytic center and is less than 8 Å away from the latter (Figure 8). This region in [NiFe]-hydrogenases appears to be very sensitive to changes. In the case of the *D. fructosovorans* hydrogenase, residue V74 in the large subunit lies in immediate proximity to T18 that is located in the small subunit at the position corresponding to W42 in the SH (Figure 8). A V74H exchange, for instance, resulted in an increased capacity of the otherwise highly oxygen-sensitive *D. fructosovorans* enzyme to perform H_2 oxidation in the presence of low O_2 concentrations.[70]

The potential roles W42 in the SH are manifold, including stabilization of the [4Fe−4S] cluster, a scaffolding function in the coordination of the postulated FMN-a cofactor, or a function as a mediator of e^- and/or H^+ transfer. However, the FMN content and the typical EPR signature of the SH were not affected by the W42S substitution, making the first two options rather unlikely. Thus, an involvement in e^-/H^+ transfer remains an appealing possibility. In fact, crucial roles of tryptophan residues in electron and proton-coupled electron transport processes have been described previously for biological[71] and semiartificial systems.[72] It should be stressed in this respect that residue W42 is present only in NAD^+-reducing [NiFe]-hydrogenases that are supposed to be O_2-tolerant. On the basis of the current model, O_2 is reductively removed from the active site most probably through reverse electron flow,[6,21−23] and, very recently, this reaction has been proposed to rely on peroxidase activity related to reversible oxygenation of noninnocent cysteine ligands of the active site.[61] In the case of the SH, NADH-derived electrons can be transferred all the way down from the NADH binding site via the [4Fe−4S] cluster in HoxY back to the active site, where O_2 attack takes place. Tryptophan 42, and probably also cysteine 39, might facilitate electron (and/or proton) transfer from the [4Fe−4S] cluster in HoxY to the active site to guarantee complete reduction of O_2.

■ ASSOCIATED CONTENT

Supporting Information

Table S1: Plasmids used in this study. Table S2: Mutagenic primers used in this study. Table S3: Overview of the characterization of the mutant strains and the isolated SH variants. Table S4: Comparison of the purified SH^{WT} and SH^{W42S}. Table S5: NAD^+ reduction activities of preparations of the SH^{C41S} complex. Figure S1: Comparison of HoxY proteins from NAD^+-reducing group 3 [NiFe]-hydrogenases with the corresponding sections of group 1 [NiFe]-hydrogenase small subunits and Complex I subunits. Figure S2: SH-based lithoautotrophic growth of mutant strains at increasing O_2 concentrations. Figure S3: SH-based lithoautotrophic growth of mutant strains missing one canonical cysteine or tryptophan W42 in the HoxY subunit of the SH. Figure S4: Verification of the HoxY and HoxH protein stability by Western blot analysis. Figure S5: Effect of FMN and DTT on the H_2-dependent NAD^+ reduction activity of the SH. Figure S6: NAD^+-dependent H_2 consumption of SH^{WT} and SH^{C39*} in the presence and absence of O_2 measured with an inverted Clark-type electrode. Figure S7: UV−visible absorption spectra of the SH^{WT} and different SH variants in the as isolated, oxidized state. Figure S8: FTIR spectra of the SH^{C39G} and SH^{C39S} variants. Figure S9: Structural implications of the W42S exchange in HoxY as revealed by FTIR difference spectroscopy. This material is available free of charge via the Internet at http://pubs.acs.org.

■ AUTHOR INFORMATION

Corresponding Author

*Phone: +49 (0)30 31425650; E-mail: oliver.lenz@tu-berlin.de.

Funding

This work is supported by the German Ministry of Science and Education (BMBF, H_2 Design Cell; to K.K. and O.L.) and the Deutsche Forschungsgemeinschaft (DFG, Cluster of Excellence "Unifying Concepts in Catalysis"; to S.W., M.H., L.L., I.Z., and O.L). K.K. received a scholarship from the Humboldt-Universität zu Berlin (Frauenförderung des Instituts für Biologie).

DOI: 10.1021/bi501347u
Biochemistry 2015, 54, 389−403

Notes

The authors declare no competing financial interest.

■ ACKNOWLEDGMENTS

Josta Hamann and Angelika Strack are acknowledged for their excellent technical assistance. We are grateful to Caspar Schäfer for providing strain HF869 and to Stefan Frielingsdorf for help with the HD exchange experiments. We would like to thank Bärbel Friedrich and Peter Hildebrandt for continuous support and helpful discussions.

■ ABBREVIATIONS

BV, benzyl viologen dichloride; CTAB, cetyltrimethylammonium bromide; DT, sodium dithionite; DTT, dithiothreitol; EPR, electron paramagnetic resonance; FMN, flavin mononucleotide; FTIR, Fourier-transform infrared:; MBH, membrane-bound [NiFe]-hydrogenase; MV, methyl viologen; SH, soluble [NiFe]-hydrogenase; TCEP, Tris(2-chlorethyl)-phosphate

■ REFERENCES

(1) Schwartz, E., Fritsch, J., and Friedrich, B. (2012) H_2-metabolizing prokaryotes, in *The Prokaryotes: Prokaryotic Physiolology and Biochemistry* (Rosenberg, E., DeLong, E., Lory, S., Stackebrandt, E., and Thompson, F., Eds.) 4th ed., pp 119−199, Springer, Berlin, Germany.

(2) Buhrke, T., Lenz, O., Krauss, N., and Friedrich, B. (2005) Oxygen tolerance of the H_2-sensing [NiFe] hydrogenase from *Ralstonia eutropha* H16 is based on limited access of oxygen to the active site. *J. Biol. Chem. 280*, 23791−23796.

(3) Liebgott, P.-P., Leroux, F., Burlat, B., Dementin, S., Baffert, C., Lautier, T., Fourmond, V., Ceccaldi, P., Cavazza, C., Meynial-Salles, I., Soucaille, P., Fontecilla-Camps, J. C., Guigliarelli, B., Bertrand, P., Rousset, M., and Léger, C. (2010) Relating diffusion along the substrate tunnel and oxygen sensitivity in hydrogenase. *Nat. Chem. Biol. 6*, 63−70.

(4) Friedrich, B., Fritsch, J., and Lenz, O. (2011) Oxygen-tolerant hydrogenases in hydrogen-based technologies. *Curr. Opin. Biotechnol. 22*, 358−364.

(5) Liebgott, P.-P., Lacey, A. L. d., Burlat, B., Cournac, L., Richaud, P., Brugna, M., Fernandez, V. M., Guigliarelli, B., Rousset, M., Léger, C., and Dementin, S. (2011) Original design of an oxygen-tolerant [NiFe] hydrogenase: major effect of a valine-to-cysteine mutation near the active site. *J. Am. Chem. Soc. 133*, 986−997.

(6) Fritsch, J., Lenz, O., and Friedrich, B. (2013) Structure, function and biosynthesis of O_2-tolerant hydrogenases. *Nat. Rev. Microbiol. 11*, 106−114.

(7) Krassen, H., Schwarze, A., Friedrich, B., Ataka, K., Lenz, O., and Heberle, J. (2009) Photosynthetic hydrogen production by a hybrid complex of photosystem I and [NiFe]-hydrogenase. *ACS Nano 3*, 4055−4061.

(8) Schwarze, A., Kopczak, M. J., Rögner, M., and Lenz, O. (2010) Requirements for construction of a functional hybrid complex of photosystem I and [NiFe]-hydrogenase. *Appl. Environ. Microbiol. 76*, 2641−2651.

(9) Vincent, K. A., Cracknell, J. A., Clark, J. R., Ludwig, M., Lenz, O., Friedrich, B., and Armstrong, F. A. (2006) Electricity from low-level H_2 in still air—an ultimate test for an oxygen tolerant hydrogenase. *Chem. Commun.*, 5033−5035.

(10) Lauterbach, L., Lenz, O., and Vincent, K. A. (2013) H_2-driven cofactor regeneration with $NAD(P)^+$-reducing hydrogenases. *FEBS J. 280*, 3058−3068.

(11) Fritsch, J., Scheerer, P., Frielingsdorf, S., Kroschinsky, S., Friedrich, B., Lenz, O., and Spahn, C. M. T. (2011) The crystal structure of an oxygen-tolerant hydrogenase uncovers a novel iron-sulphur centre. *Nature 479*, 249−252.

(12) Shomura, Y., Yoon, K.-S., Nishihara, H., and Higuchi, Y. (2011) Structural basis for a [4Fe−3S] cluster in the oxygen-tolerant membrane-bound [NiFe]-hydrogenase. *Nature 479*, 253−256.

(13) Volbeda, A., Amara, P., Darnault, C., Mouesca, J.-M., Parkin, A., Roessler, M. M., Armstrong, F. A., and Fontecilla-Camps, J. C. (2012) X-ray crystallographic and computational studies of the O_2-tolerant [NiFe]-hydrogenase 1 from *Escherichia coli*. *Proc. Natl. Acad. Sci. U.S.A. 109*, 5305−5310.

(14) Goris, T., Wait, A. F., Saggu, M., Fritsch, J., Heidary, N., Stein, M., Zebger, I., Lendzian, F., Armstrong, F. A., Friedrich, B., and Lenz, O. (2011) A unique iron−sulfur cluster is crucial for oxygen tolerance of a [NiFe]-hydrogenase. *Nat. Chem. Biol. 7*, 310−318.

(15) Lukey, M. J., Roessler, M. M., Parkin, A., Evans, R. M., Davies, R. A., Lenz, O., Friedrich, B., Sargent, F., and Armstrong, F. A. (2011) Oxygen-tolerant [NiFe]-hydrogenases: the individual and collective importance of supernumerary cysteines at the proximal Fe−S cluster. *J. Am. Chem. Soc. 133*, 16881−16892.

(16) Saggu, M., Zebger, I., Ludwig, M., Lenz, O., Friedrich, B., Hildebrandt, P., and Lendzian, F. (2009) Spectroscopic insights into the oxygen-tolerant membrane-associated [NiFe] hydrogenase of *Ralstonia eutropha* H16. *J. Biol. Chem. 284*, 16264−16276.

(17) Pandelia, M.-E., Nitschke, W., Infossi, P., Giudici-Orticoni, M.-T., Bill, E., and Lubitz, W. (2011) Characterization of a unique [FeS] cluster in the electron transfer chain of the oxygen tolerant [NiFe] hydrogenase from *Aquifex aeolicus*. *Proc. Natl. Acad. Sci. U.S.A. 108*, 6097−6102.

(18) Roessler, M. M., Evans, R. M., Davies, R. A., Harmer, J., and Armstrong, F. A. (2012) EPR spectroscopic studies of the Fe−S clusters in the O_2-tolerant [NiFe]-hydrogenase Hyd-1 from *Escherichia coli* and characterization of the unique [4Fe−3S] cluster by HYSCORE. *J. Am. Chem. Soc. 134*, 15581−15594.

(19) Pandelia, M.-E., Bykov, D., Izsak, R., Infossi, P., Giudici-Orticoni, M.-T., Bill, E., Neese, F., and Lubitz, W. (2013) Electronic structure of the unique [4Fe−3S] cluster in O_2-tolerant hydrogenases characterized by ^{57}Fe Mössbauer and EPR spectroscopy. *Proc. Natl. Acad. Sci. U.S.A. 110*, 483−488.

(20) Frielingsdorf, S., Fritsch, J., Schmidt, A., Hammer, M., Löwenstein, J., Siebert, E., Pelmenschikov, V., Jaenicke, T., Kalms, J., Rippers, Y., Lendzian, F., Zebger, I., Teutloff, C., Kaupp, M., Bittl, R., Hildebrandt, P., Friedrich, B., Lenz, O., and Scheerer, P. (2014) Reversible [4Fe−3S] cluster morphing in an O_2-tolerant [NiFe] hydrogenase. *Nat. Chem. Biol. 10*, 378−385.

(21) Lenz, O., Ludwig, M., Schubert, T., Bürstel, I., Ganskow, S., Goris, T., Schwarze, A., and Friedrich, B. (2010) H_2 conversion in the presence of O_2 as performed by the membrane-bound [NiFe]-hydrogenase of *Ralstonia eutropha*. *ChemPhysChem 11*, 1107−1119.

(22) Lauterbach, L., and Lenz, O. (2013) Catalytic production of hydrogen peroxide and water by oxygen-tolerant [NiFe]-hydrogenase during H_2 cycling in the presence of O_2. *J. Am. Chem. Soc. 135*, 17897−17905.

(23) Wulff, P., Day, C. C., Sargent, F., and Armstrong, F. A. (2014) How oxygen reacts with oxygen-tolerant respiratory [NiFe]-hydrogenases. *Proc. Natl. Acad. Sci. U.S.A. 111*, 6606−6611.

(24) Vignais, P. M., and Billoud, B. (2007) Occurrence, classification, and biological function of hydrogenases: an overview. *Chem. Rev. 107*, 4206−4272.

(25) Schneider, K., and Schlegel, H. G. (1976) Purification and properties of soluble hydrogenase from *Alcaligenes eutrophus* H 16. *Biochim. Biophys. Acta 452*, 66−80.

(26) Schneider, K., Cammack, R., and Schlegel, H. G. (1984) Content and localization of FMN, Fe−S clusters and nickel in the NAD-linked hydrogenase of *Nocardia opaca* 1b. *Eur. J. Biochem. 142*, 75−84.

(27) Lauterbach, L., Idris, Z., Vincent, K. A., and Lenz, O. (2011) Catalytic properties of the isolated diaphorase fragment of the NAD-reducing [NiFe]-hydrogenase from *Ralstonia eutropha*. *PloS one 6*, e25939.

(28) Lauterbach, L., Liu, J., Horch, M., Hummel, P., Schwarze, A., Haumann, M., Vincent, K. A., Lenz, O., and Zebger, I. (2011) The

DOI: 10.1021/bi501347u
Biochemistry 2015, 54, 389−403

hydrogenase subcomplex of the NAD$^+$-reducing [NiFe] hydrogenase from *Ralstonia eutropha*—insights into catalysis and redox interconversions. *Eur. J. Inorg. Chem. 2011*, 1067−1079.
(29) Appel, J., Phunpruch, S., Steinmüller, K., and Schulz, R. (2000) The bidirectional hydrogenase of *Synechocystis* sp. PCC 6803 works as an electron valve during photosynthesis. *Arch. Microbiol. 173*, 333−338.
(30) Gutekunst, K., Chen, X., Schreiber, K., Kaspar, U., Makam, S., and Appel, J. (2014) The bidirectional NiFe-hydrogenase in *Synechocystis* sp. PCC 6803 is reduced by flavodoxin and ferredoxin and is essential under mixotrophic, nitrate-limiting conditions. *J. Biol. Chem. 289*, 1930−1937.
(31) McIntosh, C. L., Germer, F., Schulz, R., Appel, J., and Jones, A. K. (2011) The [NiFe]-hydrogenase of the cyanobacterium *Synechocystis* sp. PCC 6803 works bidirectionally with a bias to H_2 production. *J. Am. Chem. Soc. 133*, 11308−11319.
(32) Schneider, K., Cammack, R., Schlegel, H. G., and Hall, D. O. (1979) The iron−sulphur centres of soluble hydrogenase from *Alcaligenes eutrophus*. *Biochim. Biophys. Acta 578*, 445−461.
(33) Schneider, K., and Schlegel, H. G. (1981) Production of superoxide radicals by soluble hydrogenase from *Alcaligenes eutrophus* H16. *Biochem. J. 193*, 99−107.
(34) Kömen, R., Schmidt, K., and Friedrich, B. (1992) Hydrogenase mutants of *Alcaligenes eutrophus* H16 show alterations in the electron transport system. *FEMS Microbiol. Lett. 75*, 173−178.
(35) Kuhn, M., Steinbüchel, A., and Schlegel, H. G. (1984) Hydrogen evolution by strictly aerobic hydrogen bacteria under anaerobic conditions. *J. Bacteriol. 159*, 633−639.
(36) Burgdorf, T., van der Linden, E., Bernhard, M., Yin, Q. Y., Back, J. W., Hartog, A. F., Muijsers, A. O., Koster, C. G. d., Albracht, S. P. J., and Friedrich, B. (2005) The soluble NAD$^+$-reducing [NiFe]-hydrogenase from *Ralstonia eutropha* H16 consists of six subunits and can be specifically activated by NADPH. *J. Bacteriol. 187*, 3122−3132.
(37) Horch, M., Lauterbach, L., Saggu, M., Hildebrandt, P., Lendzian, F., Bittl, R., Lenz, O., and Zebger, I. (2010) Probing the active site of an O_2-tolerant NAD$^+$-reducing [NiFe]-hydrogenase from *Ralstonia eutropha* H16 by *in situ* EPR and FTIR spectroscopy. *Angew. Chem., Int. Ed. 49*, 8026−8029.
(38) Horch, M., Lauterbach, L., Lenz, O., Hildebrandt, P., and Zebger, I. (2012) NAD(H)-coupled hydrogen cycling—structure−function relationships of bidirectional [NiFe] hydrogenases. *FEBS Lett. 586*, 545−556.
(39) Schneider, K., and Schlegel, H. G. (1978) Identification and quantitative determination of the flavin component of soluble hydrogenase from *Alcaligenes eutrophus*. *Biochem. Biophys. Res. Commun. 84*, 564−571.
(40) van der Linden, E., Faber, B. W., Bleijlevens, B., Burgdorf, T., Bernhard, M., Friedrich, B., and Albracht, S. P. J. (2004) Selective release and function of one of the two FMN groups in the cytoplasmic NAD$^+$-reducing [NiFe]-hydrogenase from *Ralstonia eutropha*. *Eur. J. Biochem. 271*, 801−808.
(41) Erkens, A., Schneider, K., and Müller, A. (1996) The NAD-linked soluble hydrogenase from *Alcaligenes eutrophus* H16: detection and characterization of EPR signals deriving from nickel and flavin. *J. Biol. Inorg. Chem. 1996*, 99−110.
(42) van der Linden, E., Burgdorf, T., Lacey, A. L. d., Buhrke, T., Scholte, M., Fernandez, V. M., Friedrich, B., and Albracht, S. P. J. (2006) An improved purification procedure for the soluble [NiFe]-hydrogenase of *Ralstonia eutropha*: new insights into its (in)stability and spectroscopic properties. *J. Biol. Inorg. Chem. 11*, 247−260.
(43) Hwang, W. C., Xu, Q., Wu, B., and Godzik, A. (2014) Crystal structure of a Baeyer-Villiger flavin-containing monooxygenase from *Staphylococcus aureus* MRSA strain MU50. *Proteins*, DOI: 10.1002/prot.24661.
(44) Simon, R., Priefer, U., and Pühler, A. (1983) A broad host range mobilization system for *in vivo* genetic engineering: transposon mutagenesis in gram negative bacteria. *Nat. Biotechnol. 1*, 784−791.
(45) Lenz, O., and Friedrich, B. (1998) A novel multicomponent regulatory system mediates H_2 sensing in *Alcaligenes eutrophus*. *Proc. Natl. Acad. Sci. U.S.A. 95*, 12474−12479.
(46) Windhövel, U., and Bowien, B. (1990) On the operon structure of the *cfx* gene clusters in *Alcaligenes eutrophus*. *Arch. Microbiol. 154*, 85−91.
(47) Pfennig, N. (1974) *Rhodopseudomonas globiformis*, sp. n., a new species of the *Rhodospirillaceae*. *Arch. Microbiol. 100*, 197−206.
(48) Friedrich, B., Heine, E., Finck, A., and Friedrich, C. G. (1981) Nickel requirement for active hydrogenase formation in *Alcaligenes eutrophus*. *J. Bacteriol. 145*, 1144−1149.
(49) Wang, R., Healey, F. P., and Myers, J. (1971) Amperometric measurement of hydrogen evolution in *Chlamydomonas*. *Plant Physiol. 48*, 108−110.
(50) Krezel, A., and Bal, W. (2004) A formula for correlating pK_a values determined in D_2O and H_2O. *J. Inorg. Biochem. 98*, 161−166.
(51) Laemmli, U. K. (1970) Cleavage of structural proteins during the assembly of the head of bacteriophage T4. *Nature 227*, 680−685.
(52) Foerstendorf, H., Mummert, E., Schäfer, E., Scheer, H., and Siebert, F. (1996) Fourier-transform infrared spectroscopy of phytochrome: difference spectra of the intermediates of the photoreactions. *Biochemistry 35*, 10793−10799.
(53) Thompson, J. D., Gibson, T. J., and Des Higgins, G. (2002) Multiple sequence alignment using ClustalW and ClustalX. *Curr. Protoc. Bioinf.*, DOI: 10.1002/0471250953.bi0203s00.
(54) Waterhouse, A. M., Procter, J. B., Martin, D. M. A., Clamp, M., and Barton, G. J. (2009) Jalview Version 2—a multiple sequence alignment editor and analysis workbench. *Bioinformatics 25*, 1189−1191.
(55) Lenz, O., Bernhard, M., Buhrke, T., Schwartz, E., and Friedrich, B. (2002) The hydrogen-sensing apparatus in *Ralstonia eutropha*. *J. Mol. Microbiol. Biotechnol. 4*, 255−262.
(56) Schäfer, C., Friedrich, B., and Lenz, O. (2013) Novel, oxygen-insensitive group 5 [NiFe]-hydrogenase in *Ralstonia eutropha*. *Appl. Environ. Microbiol. 79*, 5137−5145.
(57) van Gastel, M., Stein, M., Brecht, M., Schröder, O., Lendzian, F., Bittl, R., Ogata, H., Higuchi, Y., and Lubitz, W. (2006) A single-crystal ENDOR and density functional theory study of the oxidized states of the [NiFe] hydrogenase from *Desulfovibrio vulgaris* Miyazaki F. *J. Biol. Inorg. Chem. 11*, 41−51.
(58) Brecht, M., van Gastel, M., Buhrke, T., Friedrich, B., and Lubitz, W. (2003) Direct detection of a hydrogen ligand in the [NiFe] center of the regulatory H_2-sensing hydrogenase from *Ralstonia eutropha* in its reduced state by HYSCORE and ENDOR spectroscopy. *J. Am. Chem. Soc. 125*, 13075−13083.
(59) Lacey, A. L. d., Fernandez, V. M., Rousset, M., and Cammack, R. (2007) Activation and inactivation of hydrogenase function and the catalytic cycle: spectroelectrochemical studies. *Chem. Rev. 107*, 4304−4330.
(60) Happe, R. P., Roseboom, W., Egert, G., Friedrich, C. G., Massanz, C., Friedrich, B., and Albracht, S. P. (2000) Unusual FTIR and EPR properties of the H_2-activating site of the cytoplasmic NAD-reducing hydrogenase from *Ralstonia eutropha*. *FEBS Lett. 466*, 259−263.
(61) Horch, M., Lauterbach, L., Mroginski, M. A., Hildebrandt, P., Lenz, O., and Zebger, I. (2015) Reversible active site sulfoxygenation can explain the oxygen tolerance of a NAD$^+$-reducing [NiFe] hydrogenase and its unusual infrared spectroscopic properties, submitted for publication.
(62) Cuello, A. O., McIntosh, C. M., and Rotello, V. M. (2000) Model systems for flavoenzyme activity. The role of N_3−H hydrogen bonding in flavin redox processes. *J. Am. Chem. Soc. 122*, 3517−3521.
(63) Breinlinger, E. C., Keenan, C. J., and Rotello, V. M. (1998) Modulation of flavin recognition and redox properties through donor atom−π interactions. *J. Am. Chem. Soc. 120*, 8606−8609.
(64) Kao, Y.-T., Saxena, C., He, T.-F., Guo, L., Wang, L., Sancar, A., and Zhong, D. (2008) Ultrafast dynamics of flavins in five redox states. *J. Am. Chem. Soc. 130*, 13132−13139.

DOI: 10.1021/bi501347u
Biochemistry 2015, 54, 389−403

(65) Lans, I., Frago, S., and Medina, M. (2012) Understanding the FMN cofactor chemistry within the *Anabaena* flavodoxin environment. *Biochim. Biophys. Acta 1817*, 2118−2127.
(66) Grzeszik, C., Lübbers, M., Reh, M., and Schlegel, H. G. (1997) Genes encoding the NAD-reducing hydrogenase of *Rhodococcus opacus* MR11. *Microbiology 143*, 1271−1286.
(67) Zaborosch, C., Köster, M., Bill, E., Schneider, K., Schlegel, H. G., and Trautwein, A. X. (1995) EPR and Mössbauer spectroscopic studies on the tetrameric, NAD-linked hydrogenase of *Nocardia opaca* 1b and its two dimers: 1. The *βδ*-dimer—a prototype of a simple hydrogenase. *Biometals 8*, 149−162.
(68) Ogata, H., Hirota, S., Nakahara, A., Komori, H., Shibata, N., Kato, T., Kano, K., and Higuchi, Y. (2005) Activation process of [NiFe] hydrogenase elucidated by high-resolution X-ray analyses: conversion of the ready to the unready state. *Structure 13*, 1635−1642.
(69) Germer, F., Zebger, I., Saggu, M., Lendzian, F., Schulz, R., and Appel, J. (2009) Overexpression, isolation, and spectroscopic characterization of the bidirectional [NiFe] hydrogenase from *Synechocystis* sp. PCC 6803. *J. Biol. Chem. 284*, 36462−36472.
(70) Abou Hamdan, A., Dementin, S., Liebgott, P. P., Gutierrez-Sanz, O., Richaud, P., De Lacey, A. L., Rousset, M., Bertrand, P., Cournac, L., and Leger, C. (2012) Understanding and tuning the catalytic bias of hydrogenase. *J. Am. Chem. Soc. 134*, 8368−8371.
(71) Shih, C., Museth, A. K., Abrahamsson, M., Blanco-Rodriguez, A. M., Di Bilio, A. J., Sudhamsu, J., Crane, B. R., Ronayne, K. L., Towrie, M., Vlcek, A., Richards, J. H., Winkler, J. R., and Gray, H. B. (2008) Tryptophan-accelerated electron flow through proteins. *Science 320*, 1760−1762.
(72) Sancar, A. (2003) Structure and function of DNA photolyase and cryptochrome blue-light photoreceptors. *Chem. Rev. 103*, 2203−2238.
(73) Kortlüke, C., and Friedrich, B. (1992) Maturation of membrane-bound hydrogenase of *Alcaligenes eutrophus* H16. *J. Bacteriol. 174*, 6290−6293.
(74) Sambrook, J., Fritsch, E. F., and Maniatis, T. (1989) *Molecular Cloning: A Laboratory Manual*, 2nd ed., Cold Spring Harbor Laboratory, Cold Spring Harbor, NY.

DOI: 10.1021/bi501347u
Biochemistry 2015, 54, 389−403